



Climate and Ecosystem Sciences Division



---

29 May 2018

Dennis Baldocchi, Siyan Ma, and Joseph Verfaillie  
Department of Environmental Science, Policy, and Management  
University of California, Berkeley

Dear Dennis, Siyan, and Joe

Thank you very much for hosting the AmeriFlux Tech team site visit at the Vaira Ranch site (US-Var) from 10 – 24 April 2017 (DOY 100 - 114). This report summarizes the findings and key recommendations from the comparison between the AmeriFlux portable eddy covariance system #2 (PECS2) and the *in situ* system for eddy covariance, radiation, and meteorological observations.

The AmeriFlux PECS2 sensors were deployed to minimize separation (both horizontal and vertical) from the *in situ* sensors (Appendix 1), to avoid interfering with existing infrastructure, and to prevent shadowing or wake effects. The AmeriFlux PECS2 was deployed with two infrared gas analyzer (an enclosed-path - LI-7200, and an open-path analyzer - LI-7500A). Both gas analyzers are calibrated prior to and checked after each deployment, with this comparison focusing on the AmeriFlux open-path IRGA as it is similar to the *in situ* CO<sub>2</sub> eddy covariance system. Data processing of the AmeriFlux PECS2 data was handled by EddyPro® (Version 6.2.0), an open-source eddy covariance software package developed by LI-COR ([http://licor.com/env/products/eddy\\_covariance/software.html](http://licor.com/env/products/eddy_covariance/software.html)). Please contact the AmeriFlux Tech team if you have specific questions.

Four figures are generated for each variable compared. The top figure is a time series of both systems over the evaluation period. The middle figure is a time series of the differences between the two systems. The lower left figure is a scatter plot of both systems with the ideal 1 to 1 regression line and the best fit orthogonal regression together with equation and fit parameters. Lastly, the lower right figure is a histogram of the differences between the systems with summary statistics. The enclosed figures only include periods where both datasets are available and quality controlled. Missing data periods occurred when data was screened from one or both systems either through data quality checks, outlier removal, environmental interference (precipitation), or no data (power outage) (Figure 1).

### **Key Recommendations:**

Overall, the comparison between the AmeriFlux PECS2 and the *in situ* system was relatively good. Please see a few key findings highlighted below:

- There were differences in the covariance of vertical wind and CO<sub>2</sub>, with *in situ* values reading over 30% lower values. We found the covariance to be identical to the CO<sub>2</sub> fluxes suggesting that a density correction was included. This was previously observed in the report for Tonzi Ranch (US-Ton). We recommend covariances to be reported without additional corrections.
- Highest discrepancies in radiation values were observed in the incoming and outgoing longwave radiation components. The *in situ* readings were higher than those of the PECS2 CNR4, possibly due to differences in sensor body temperature. We recommend investigating these readings, or servicing the radiometer and verifying that the body temperature values are accurate and are being applied correctly in estimating true longwave radiation.
- Incoming and reflected PAR *in situ* values deviated only by a few percent when comparing to the PECS2 quantum probes. Though a small percentage these resulted in over 100 μmol m<sup>-2</sup> s<sup>-1</sup> in absolute terms under sunny conditions.

Summarizing, we emphasize regular calibration checks and following the manufacturer's recommendations for routine maintenance (factory calibration, cleaning instrumentation, changing internal chemicals, etc.) of gas analyzer and meteorological sensors, and the verification of the implemented conversion and calibration factors when converting to physical units.

Note that the AmeriFlux Tech team provides calibration gases (check and span gases) as well as calibrated PAR sensors at no cost to active AmeriFlux sites, to conduct their own calibrations.

In closing, thank you for your cooperation before, during, and after the site visit and we encourage you to continue your active participation in the AmeriFlux network. We are actively soliciting comments or feedback regarding the site visit process and report to maximize the utility of our visits. For all reports, we request a summary from the site PI to describe how the enclosed recommendations will be addressed. We are available to provide further analysis or discussion of the results, if necessary. Please review the general site information table in Appendix 1 of this document and let us know if you notice erroneous information. Thank you for working collaboratively with the AmeriFlux Tech team.

All the best,

Sigrid Dengel<sup>1</sup>, Stephen Chan<sup>1</sup>, Sébastien Biraud<sup>1</sup>, David Billesbach<sup>2</sup>, Chad Hanson<sup>3</sup>

AmeriFlux Tech team

<sup>1</sup>Lawrence Berkeley National Laboratory

<sup>2</sup>University of Nebraska, Lincoln

<sup>3</sup>Oregon State University

## Detailed Report

### Data availability:

The PECS2 was deployed from 10 – 24 April 2017 (Figure 1) with observations spanning a total of 13 full days with the assessment concentrating on the comparison between PECS2 and the already existing *in situ* EC setup. A few periods of data were excluded from the analysis when the PECS2 leaf wetness sensor (LWS) recorded periods of rain or dew affecting the performance of sonic anemometers, the open-path gas analyzer signal strength and gas mole density readings (Burba, 2013). These time periods are highlighted in Figure 1, together with the overall data availability.

### Data processing:

The site staff provided 30-minute processed data and the raw 10 Hz data from the *in situ* eddy flux system. The AmeriFlux Tech Team independently processed these data using EddyPro Version 6.2.0 (see Figure 2) to confirm data processing procedures and understand where discrepancies originate from. Since the *in situ* staff is not applying any high nor low frequency corrections to their flux calculations, we followed similar steps to avoid unnecessary discrepancies. That said, we were only able to match these timeseries once we applied a fixed lag time value of +0.2 seconds and reduced the despiking threshold for vertical wind to 3 standard deviations (Figure 2). There was very good agreement between *in situ* and independently processed fluxes for CO<sub>2</sub> (slope: 1.00, offset: -0.01 μmol m<sup>-2</sup> s<sup>-1</sup>, R<sup>2</sup> = 1.00), latent heat (slope: 1.00, offset: -0.06 W m<sup>-2</sup>, R<sup>2</sup> = 1.00) and sensible heat flux (slope: 1.00, offset: +0.14 W m<sup>-2</sup>, R<sup>2</sup> = 1.00) (Figure 2). Including the Massman (2000, 2001) spectral correction and comparing the independently calculated fluxes (including and excluding the spectral correction), we see a difference of 14% in CO<sub>2</sub> and 8% in latent heat fluxes indicating a notable loss in these final fluxes. Since excluding any spectral corrections is the standard procedure for this site, the PECS2 data was processed similarly.

Noticeable discrepancies were found in the covariance between vertical wind and CO<sub>2</sub> where we saw a difference of over 30% (Figure 3) when comparing PECS2 data with *in situ* data. We found that the *in situ* covariance was identical to the final flux (see Figure 7 and Figure 8) which suggested that the reported covariance included the density correction term.

Site Name: Vaira Ranch – lone (US-Var)

Visit Dates: 10 – 24 April 2017

We made a similar observation at Tonzi (please see report from the Tonzi Ranch, 2016) and recommend reported covariances not to include any additional corrections. The covariance between vertical wind and water vapor matched much more closely although some skewness in the distribution of differences remained (Figure 4, slope: 0.96, offset: +0.02 ( $\text{mmol m}^{-2} \text{s}^{-1}$ )<sup>2</sup>,  $R^2 = 1.00$ ) as can also be seen in the covariance between vertical wind and sonic temperature that was 9% higher than those estimated by the site staff (Figure 5, slope: 1.09, offset: +0.00 ( $\text{m s}^{-1} \text{ } ^\circ\text{C}$ )<sup>2</sup>,  $R^2 = 0.99$ ).

In the report figures, site processed data are labeled “in situ”, PECS2 (open-path) data (excluding spectral correction and using a 3 standard deviation despiking threshold for vertical wind) are labeled “PECSnoS+t3” and the *in situ* independently processed data by the AmeriFlux Tech team (excluding spectral corrections) as “VARLi75noS+0.2t3”. Inclusion of all or exclusion of one or the other time series (mainly when reproduced time series are identical) from particular figures are done where relevant/appropriate.

#### **Turbulent fluxes:**

Carbon dioxide fluxes exhibited a rather good agreement (Figure 6, slope: 0.95, offset: +0.14  $\mu\text{mol m}^{-2} \text{s}^{-1}$ ,  $R^2 = 0.91$ ) but showing some degree of scatter mirrored in the coefficient of determination. Regarding the covariances between vertical wind and  $\text{CO}_2$  we saw significant differences of 30% when comparing PECS2 data with *in situ* provided data (Figure 7 (in blue), slope: 0.70, offset: +0.00  $\mu\text{mol m}^{-2} \text{s}^{-1}$ ,  $R^2 = 0.91$ ) but a very good agreement between PECS2 and the independently calculated values (Figure 7 (in red), slope: 0.98, offset: +0.00  $\mu\text{mol m}^{-2} \text{s}^{-1}$ ,  $R^2 = 0.93$ ). We found that the *in situ* covariance was identical to the final flux (Figure 8) which suggested that the reported covariance included the density correction term.

Regarding latent heat, we saw 8% differences between the two open-path EC systems (Figure 9, slope: 0.92, offset: +1.12  $\text{W m}^{-2}$ ,  $R^2 = 0.97$ ), with a difference of up to 50  $\text{W m}^{-2}$  during midday hours. The covariance between *in situ* and PECS2 values correspond rather well (Figure 10 (in blue), slope: 0.97, offset: +0.01  $\text{mmol m}^{-2} \text{s}^{-1}$ ,  $R^2 = 0.97$ ) while those independently estimated diverted by 8% as well (Figure 10 (in red), slope: 0.92, offset: +0.03  $\text{mmol m}^{-2} \text{s}^{-1}$ ,  $R^2 = 0.97$ ).

Site Name: Vaira Ranch – Lone (US-Var)

Visit Dates: 10 – 24 April 2017

Since no spectral corrections were applied to the data these discrepancies in latent heat possibly result from the cumulative effect of slightly different standard deviations for water vapor, data processing and individual terms included in the density correction applied to the raw covariances.

At the same time sensible heat showed a positive deviation of 8% between PECS2 and Vaira site data (Figure 11, slope: 1.08, offset:  $-2.06 \text{ W m}^{-2}$ ,  $R^2 = 0.93$ ), while the covariance between vertical wind and the sonic temperature (Figure 12 (in blue), slope: 0.97, offset:  $-0.00 \text{ W m}^{-2}$ ,  $R^2 = 0.94$ ) showed a deviation of 3% with the *in situ* data showing lower values. Simultaneously independently estimated covariances show similar values as those observed in final sensible heat fluxes (Figure 12 (in red), slope: 1.06, offset:  $-0.00 \text{ W m}^{-2}$ ,  $R^2 = 0.94$ ). Having said this, the variances/standard deviations of the individual flux components agree well in their respective comparison.

Friction velocity values show a difference of 4% (Figure 13, slope: 1.04, offset:  $-0.00 \text{ m s}^{-1}$ ,  $R^2 = 0.88$ ) including some scatter reflected in the low coefficient of determination ( $R^2$ ). Many periods of low turbulence were observed translating the 6% difference into differences of around 10% in absolute terms (see middle panel Figure 13). Adding Figure 14 we see low turbulence periods to dominate under easterly winds.

To place the results in the context of the broader AmeriFlux network, we selected the gas and energy fluxes to benchmark (Figure 15) against the accumulated record of AmeriFlux site visits carried out between 2002 and 2012 (Schmidt *et al.*, 2012). To accomplish this, we changed the reference value from a site maximum (equation 1, see Schmidt *et al.*, 2012) to a fixed value (see Figure 15). The resulting relative instrumental error (*sensu* Schmidt *et al.*, 2012 and Figure 15 (current report)) represents the combined error originating from systematic (site dependent; instrumental, etc.) and random (combined site and PECS2; instrumental noise, change in ambient/environmental conditions, etc.) errors. Negative RIE values indicate that on average the *in situ* system has recorded lower values than PECS2 and vice versa. RIE values for variables derived from a single instrument requiring little additional corrections are usually smaller than amalgamated variables, such as final corrected fluxes, for example.

Site Name: Vaira Ranch – Ione (US-Var)

Visit Dates: 10 – 24 April 2017

The ensemble averaged (co-)spectra from independently processed data for relevant terms recorded with the open-path systems, under dry conditions only, are provided in Figure 16 and Figure 17, respectively. The spectra (Figure 16) correspond well with the *in situ* sonic temperature showing aliasing in the higher frequencies, something that was also observed in the PECS2 scalars in the highest frequency domain. Sonic aliasing affects the spectra and co-spectra but should not affect the end fluxes or variance *per se* (Massman, 2000). Relevant (co-)spectra followed each other seamlessly (Figure 17), though showing some loss in the higher frequency. This can possibly be attributed to the different data treatment and application of the vertical wind despiking threshold.

#### **IRGA scalars and statistics:**

The overall CO<sub>2</sub> mole density (Figure 18, slope 0.99, offset: +0.07 mmol m<sup>-3</sup>, R<sup>2</sup> = 1.00) estimated from open-path measurements, agreed very well showing a minimal offset of 0.14 mmol m<sup>-3</sup>. The independently calculated CO<sub>2</sub> standard deviations agreed rather well too (Figure 19 in red, slope 0.96, offset: +0.00 mmol m<sup>-3</sup>, R<sup>2</sup> = 0.97), *In situ* values showed similar agreement (Figure 19 in blue), though values appeared slightly lower. The same observation was made in water vapor as these agreed well too (Figure 20, slope 0.98, offset: +15.10 mmol m<sup>-3</sup>, R<sup>2</sup> = 0.99) with a slight offset, as did the resulting standard deviation (Figure 21, slope 0.99, offset: -0.27 mmol m<sup>-3</sup>, R<sup>2</sup> = 0.99), again in its native mole density unit. Water vapor standard deviations diverted by 5% when independently processed, as can be seen in Figure 21 (slope 0.95, offset: +0.15 mmol m<sup>-3</sup>, R<sup>2</sup> = 0.99).

#### **Sonic wind components and temperature:**

The wind direction estimated with the two sonic anemometers deviated by several degrees (Figure 22, slope: 1.02, offset: +27.34 °, R<sup>2</sup> = 1.00) that is attributed to the misorientation of the PECS2 sonic anemometer, as the independent estimated site values correspond to those provided by site staff. That said, the mean horizontal wind speed comparison from the sonic anemometers was rather good (Figure 23, slope: 1.04, offset: -0.05 m s<sup>-1</sup>, R<sup>2</sup> = 0.98). Figure 24 shows the distinctive diurnal wind distribution for the entire site visit duration (full days only) with lowest wind speeds during nighttime mostly originating from North-easterly direction.

Site Name: Vaira Ranch – lone (US-Var)

Visit Dates: 10 – 24 April 2017

Figure 25 illustrates the averaged footprint distribution estimated from PECS2 data for the entire site visit duration using the Kormann and Meixner (2001) model. As periods with low friction velocities were filtered out the footprint distribution mirrors the distinctive wind direction distribution during daytime hours (see Figure 24).

The standard deviations of the rotated wind components agreed very well (Figure 26 - Figure 28) with differences of only up to  $\pm 3\%$ . From our experience, the Gill R3-50 used on the PECS2 does not measure absolute sonic temperature very well. Our current comparison showed a difference of approximately 2 °C and exceeding once 4 °C (Figure 29, slope: 0.81, offset: +5.08,  $R^2 = 0.96$ ) with the *in situ* anemometer showing a much smaller amplitude, while standard deviation values agreed much better (Figure 30, slope: 1.03, offset: +0.01 °C,  $R^2 = 0.94$ ) with occasional scatter.

#### **Meteorological and radiation measurements:**

Air temperature measurements reported by the PECS2 HMP155 and *in situ* HMP45 sensors agreed well (Figure 31, slope: 1.04, offset: -0.17 °C,  $R^2 = 1.00$ ) with occasional diurnal fluctuations of slightly higher than 1°C during daytime hours. Adding ambient air temperature measured with the aspirated RM Young probe (PECS2) we see the *in situ* probe to over-report ambient values. Relative humidity values measured with the same devices differed more than 5% over the course of a day in absolute terms (Figure 33, slope: 1.07, offset: +5.95 %,  $R^2 = 0.99$ ) with the highest discrepancies under wet conditions (see Figure 1). We recommend following manufacturer's instrument service and calibration frequency. The atmospheric pressure measurements tracked closely (Figure 34, slope: 1.03, offset: -2.60 kPa,  $R^2 = 1.00$ ).

The incoming shortwave radiation from the *in situ* CNR1 radiometer traced the PECS2 incoming radiation relatively well (Figure 35, slope: 1.04, offset: -1.14 W m<sup>-2</sup>,  $R^2 = 1.00$ ) though showing around 40 W m<sup>-2</sup> higher values on clear days. Outgoing shortwave radiation also showed a very good agreement (Figure 36, slope: 1.00, offset: -0.45 W m<sup>-2</sup>,  $R^2 = 1.00$ ) with a deviation of  $\pm 5$  W m<sup>-2</sup> mainly during midday, that could possibly be attributed to a slight tilt as a similar trend is being observed in the incoming component. Both incoming and outgoing longwave radiation measured with the *in situ* CNR1 showed higher values than those recorded with the PECS2 CNR4 radiometer.

Site Name: Vaira Ranch – lone (US-Var)

Visit Dates: 10 – 24 April 2017

While outgoing longwave radiation showed a clear offset of around  $18 \text{ W m}^{-2}$  (Figure 39, slope: 1.00, offset:  $+18.68 \text{ W m}^{-2}$ ,  $R^2 = 0.99$ ), incoming longwave radiation showed a less organized pattern (Figure 37, slope: 1.04, offset:  $+3.55 \text{ W m}^{-2}$ ,  $R^2 = 0.94$ ). This apparent chaotic pattern disappeared once periods with rain, dew or condensation were removed from the time series (Figure 38). The CNR1 radiometer applies one coefficient to all four radiation components and can therefore be excluded as an explanation for the distinctive offset in longwave radiation. A more plausible explanation could be the differences in sensor body temperature (no data provided by *in situ* staff) and the application/integration of it. While these cancel each other out in net terms, they do not affect overall net radiation values. Nevertheless, we recommend investigating these readings as they over-report the individual longwave measurements and possibly envisage sending the radiometer in for service and/or calibration.

The comparison between the PECS2 CNR4 and the *in situ* NR Lite net radiation (Figure 40, slope: 1.09, offset:  $-11.43 \text{ W m}^{-2}$ ,  $R^2 = 0.99$  and Figure 41) showed a difference of 9%. Net radiation from the CNR1 measurements had much closer agreement between the PECS2 CNR4 radiometer (Figure 41, slope: 1.04, offset:  $-2.99 \text{ W m}^{-2}$ ,  $R^2 = 0.99$ ). The different field of view of the outgoing components possibly contributed to the observed differences.

Incoming photosynthetic active radiation (PAR) from the *in situ* PQS1 the PECS2 PQS1 (both, Kipp & Zonen) sensors agreed well with around  $100 \mu\text{mol m}^{-2} \text{ s}^{-1}$  deviations on days with high radiation (Figure 42, slope: 1.04, offset:  $-1.87 \mu\text{mol m}^{-2} \text{ s}^{-1}$ ,  $R^2 = 1.00$ ). Reflected *in situ* PAR readings (Figure 43, slope: 1.13, offset:  $-0.36 \mu\text{mol m}^{-2} \text{ s}^{-1}$ ,  $R^2 = 0.99$ ) appear to over-report radiation values by 13% mainly on days with very high reflected values, a possible indication of instrument drift/degradation as values converge under lower radiation level. Another possible origin of the divergence is the different field of view.

#### References:

Billesbach, D. P. (2011), Estimating uncertainties in individual eddy covariance flux measurements: A comparison of methods and a proposed new method, *Agric. For. Meteorol.* 151, 394–405, doi:10.1016/j.agrformet.2010.12.001.

Site Name: Vaira Ranch – Ione (US-Var)

Visit Dates: 10 – 24 April 2017

Burba, G. (2013), Eddy covariance method for scientific, industrial, agricultural and regulatory applications: A field book on measuring ecosystem gas exchange and areal emission rates.

LI-Cor Biosciences.

Finkelstein, P. L., and P. F. Sims (2001), Sampling error in eddy correlation flux measurements, *J. Geophys. Res.*, 106(D4), 3503–3509, doi:10.1029/2000JD900731.

Kormann, R., and Meixner, F. X. (2001), An analytical footprint model for non-neutral stratification. *Boundary-Layer Meteorology*, 99(2), 207-224.

Massman, W. J. (2000). A simple method for estimating frequency response corrections for eddy covariance systems. *Agricultural and Forest Meteorology*, 104(3), 185-198.

Schmidt, A., C. Hanson, W. S. Chan, and B. E. Law (2012), Empirical assessment of uncertainties of meteorological parameters and turbulent fluxes in the AmeriFlux network, *J. Geophys. Res.*, 117, G04014, doi:10.1029/2012JG002100.

**Table of Figures:**

Figure 1 – Data availability for the Vaira grassland site visit period. Periods were flagged due to system outages or poor signal. “LWS” illustrates times when the leaf wetness sensor recorded wet periods (a) affecting open-path measurements, be it rain or dew. Overall data availability for PECS2 and *in situ* are illustrated in panel b. .... 10

Figure 2 – *In situ* (“in situ”) data against independently processed *in situ* raw data (“in situ AF (noS) by the AmeriFlux Tech team, whereby “noS” stands for no high frequency spectral correction applied. Data distributions along the ideal 1:1 line (interrupted grey line) visualize the grade of reproduction. Values marked as “in situ AF” represent *in situ* values independently processed by the AmeriFlux team, including the Massman (2000) high frequency spectral correction. As illustrated some variables we were able to reproduce while other proved to be more challenging. .... 11

Figure 3 – Covariance between vertical wind and CO<sub>2</sub> measured with the LI-7500 open-path (in situ) and LI-7500A (PECS2) together with the independently processed *in situ* data (VARLi75noS+0.2t3). .... 12

Figure 4 – Covariance between vertical wind and H<sub>2</sub>O measured with the LI-7500 open-path (in situ) and LI-7500A (PECS2) together with the independently processed *in situ* data (VARLi75noS+0.2t3). .... 13

Figure 5 – Covariance between vertical wind and sonic temperature measured with the LI-7500 open-path (in situ) and LI-7500A (PECS2) together with the independently processed *in situ* data (VARLi75noS+0.2t3). .... 14

Figure 6 - CO<sub>2</sub> fluxes measured with the LI-7500 open-path (in situ) and LI-7500A (PECS2) together with the independently processed *in situ* data (VARLi75noS). .... 15

Figure 7 - Covariance of vertical wind and CO<sub>2</sub> measured with the open-path gas analyzers. “PECSnoS” represents PECS2 LI-7500A data and, “in situ”, those provided by site staff while “VARLi75noS” those independently processed data by the AmeriFlux Tech team. .... 16

Figure 8 – Comparison between the covariance of vertical wind and CO<sub>2</sub> against final CO<sub>2</sub> fluxes measured with the open-path gas analyzers. .... 17

Figure 9 - Latent heat fluxes. “PECS” represents PECS2 data, “in situ” provided by site staff, while “VARLi75” *in situ* independently processed data by the AmeriFlux Tech team. .... 18

Figure 10 – Covariance of vertical wind and water vapor. .... 19

Figure 11 – Sensible heat flux. .... 20

Figure 12 – Covariance of vertical wind and sonic temperature calculated from data recorded with the PECS2 Gill R3-50 and the *in situ* Gill WindMaster. .... 21

Figure 13 – Friction velocity. .... 22

Figure 14 – Friction velocity according to wind direction calculated from PECS2 data. .... 23

Figure 15 – Histogram of relative instrumental error (RIE) for 4 selected variables based on the accumulated record of AmeriFlux site visits. Colored bar denotes the RIE from this site visit (bar width = 5%). Laplace distribution illustrated in solid red line. Dashed, vertical lines denote mean ± √2β, where β is a scale parameter describing the Laplace distribution. The term √2β is equivalent to the standard deviation in a normal distribution. Negative RIE values indicate that on average the in situ system has recorded lower values than PECS2 (in this case) and vice versa. .... 24

Figure 16 – Ensemble averaged spectra for the open-path systems during dry periods. ....	25
Figure 17 – Ensemble averaged co-spectra for the open-path systems during dry periods. ....	26
Figure 18 – CO <sub>2</sub> mole density. ....	27
Figure 19 – Standard deviation of CO <sub>2</sub> mole density. ....	28
Figure 20 – Water vapor mole density. ....	29
Figure 21 – Standard deviation of water vapor mole density. ....	30
Figure 22 – Wind direction comparison between PECS2 and <i>in situ</i> data. The high discrepancy is attributed to the misorientation of the PECS sonic anemometer. ....	31
Figure 23 – Wind speed. ....	32
Figure 24 – Wind speed according to wind direction (represented by directional arrows) for the site visit duration (full days only), estimated from <i>in situ</i> data. Black arrows represent missing CO <sub>2</sub> flux values. ...	33
Figure 25 – Averaged footprint distribution (Kormann & Meixner, 2001) for the entire site visit measurement period, excluding periods with low turbulence values ( $u^* < 0.2$ ). ....	34
Figure 26 – Standard deviation of the rotated u-wind component. ....	35
Figure 27 – Standard deviation of the rotated v-wind component. ....	36
Figure 28 – Standard deviation of the rotated w-wind component. ....	37
Figure 29 – Mean sonic temperature. ....	38
Figure 30 – Standard deviation of the sonic temperature distribution. ....	39
Figure 31 – Ambient air temperature measured with the PECS2 HMP155 and the <i>in situ</i> HMP45 temperature and relative humidity probes. ....	40
Figure 32 – Ambient air temperature measured with the PECS2 HMP155 and the <i>in situ</i> HMP45 temperature and relative humidity probes together with the PECS2 RM Young aspirated temperature probe. ....	41
Figure 33 – Relative humidity measured with the PECS2 HMP155 and the <i>in situ</i> HMP45 temperature and relative humidity probes. ....	42
Figure 34 – Atmospheric pressure. ....	43
Figure 35 – Incoming shortwave radiation measured with the PECS2 CNR4 and the <i>in situ</i> CNR1. ....	44
Figure 36 – Outgoing shortwave radiation measured with the PECS2 CNR4 and the <i>in situ</i> CNR1. ....	45
Figure 37 – Incoming longwave radiation measured with the PECS2 CNR4 and the <i>in situ</i> CNR1. ....	46
Figure 38 – Incoming longwave radiation measured with the PECS2 CNR4 and the <i>in situ</i> CNR1, separated by weather conditions. Regression line and statistics in the right panel apply to the rain filtered data. ....	47
Figure 39 – Outgoing longwave radiation measured with the PECS2 CNR4 and the <i>in situ</i> CNR1. ....	48
Figure 40 – Net radiation measured with the PECS2 CNR4 and the <i>in situ</i> NR Lite. ....	49
Figure 41 – Net radiation measured with the PECS2 CNR4 and the <i>in situ</i> NR Lite and the <i>in situ</i> CNR1 together with the rain filtered values. Both orthogonal regression lines and statistics apply to the rain filtered data. ....	50
Figure 42 – Incoming photosynthetically active radiation (PAR). ....	51
Figure 43 – Outgoing photosynthetically active radiation (PAR). ....	52

Site Name: Vaira Ranch – Ione (US-Var)

Visit Dates: 10 – 24 April 2017

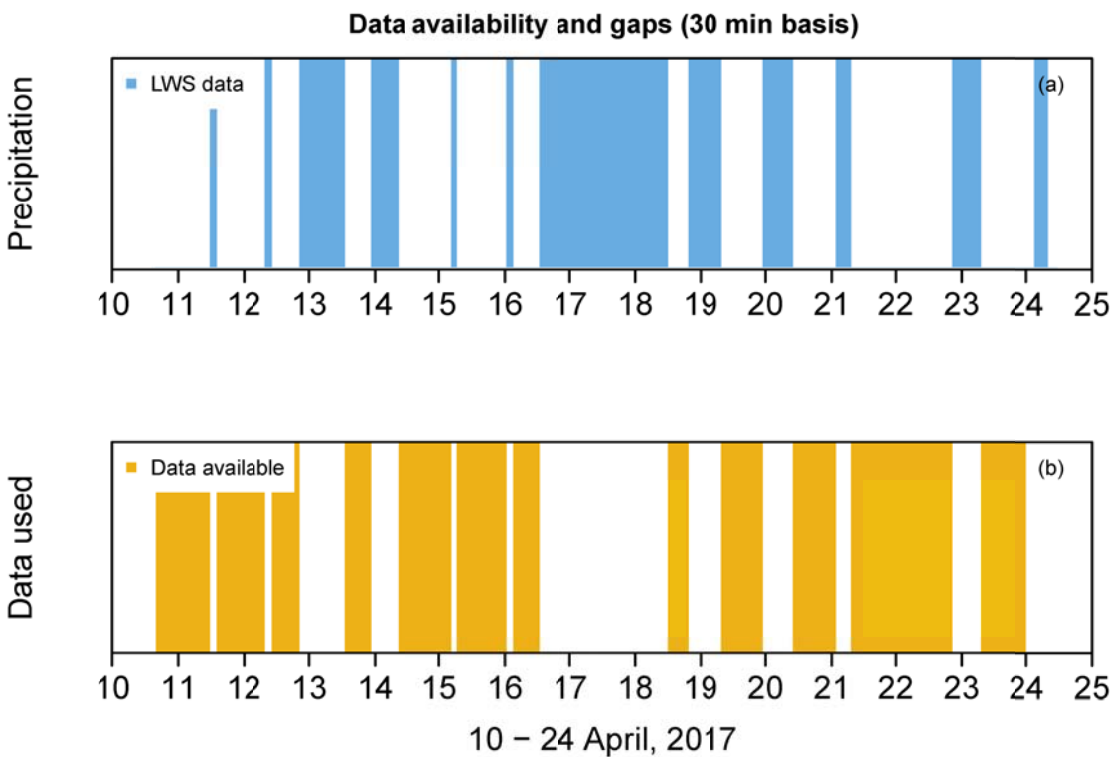


Figure 1 – Data availability for the Vaira grassland site visit period. Periods were flagged due to system outages or poor signal. “LWS” illustrates times when the leaf wetness sensor recorded wet periods (a) affecting open-path measurements, be it rain or dew. Overall data availability for PECS2 and *in situ* are illustrated in panel b.

Site Name: Vaira Ranch – Ione (US-Var)

Visit Dates: 10 – 24 April 2017

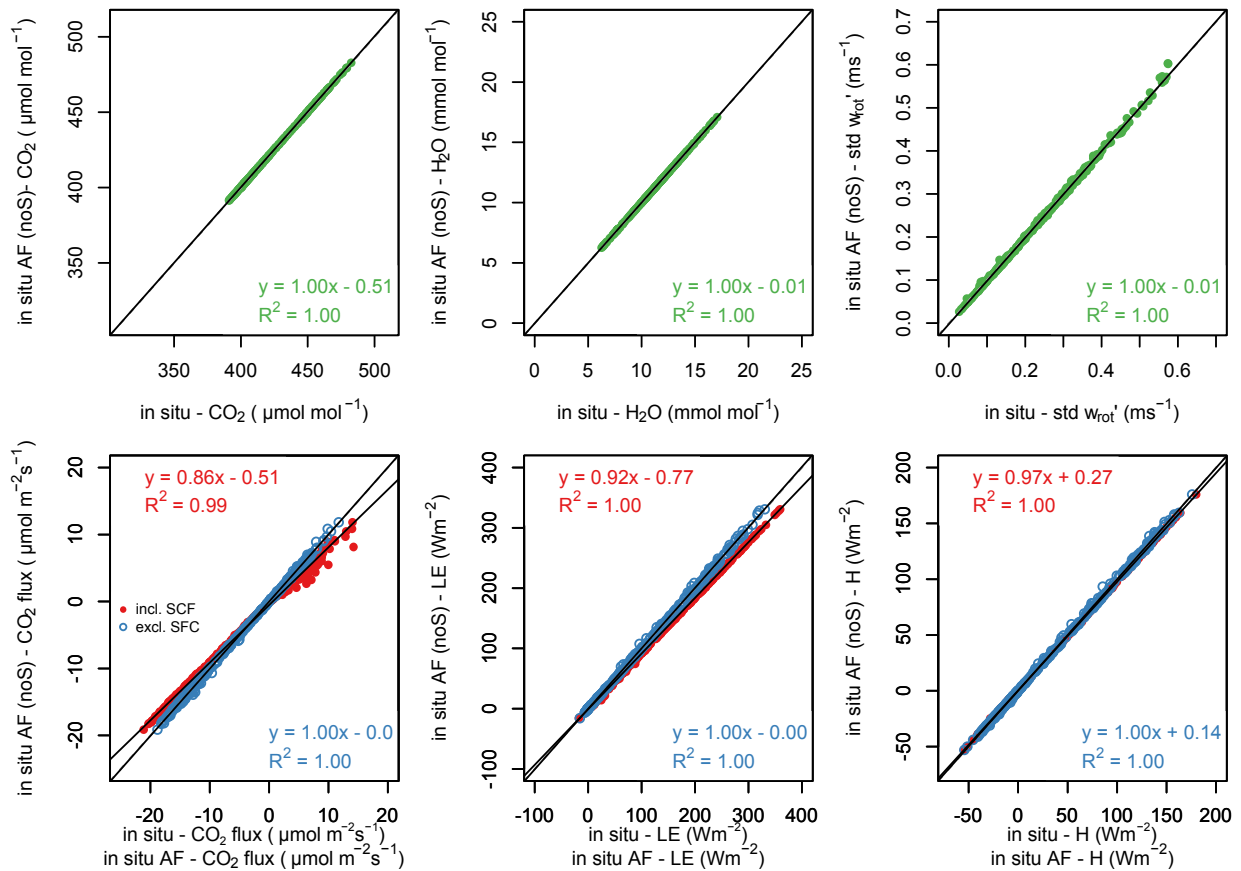


Figure 2 – *In situ* (“in situ”) data against independently processed *in situ* raw data (“in situ AF (noS)”) by the AmeriFlux Tech team, whereby “noS” stands for no high frequency spectral correction applied. Data distributions along the ideal 1:1 line (interrupted grey line) visualize the grade of reproduction. Values marked as “in situ AF” represent *in situ* values independently processed by the AmeriFlux team, including the Massman (2000) high frequency spectral correction. As illustrated some variables we were able to reproduce while other proved to be more challenging.

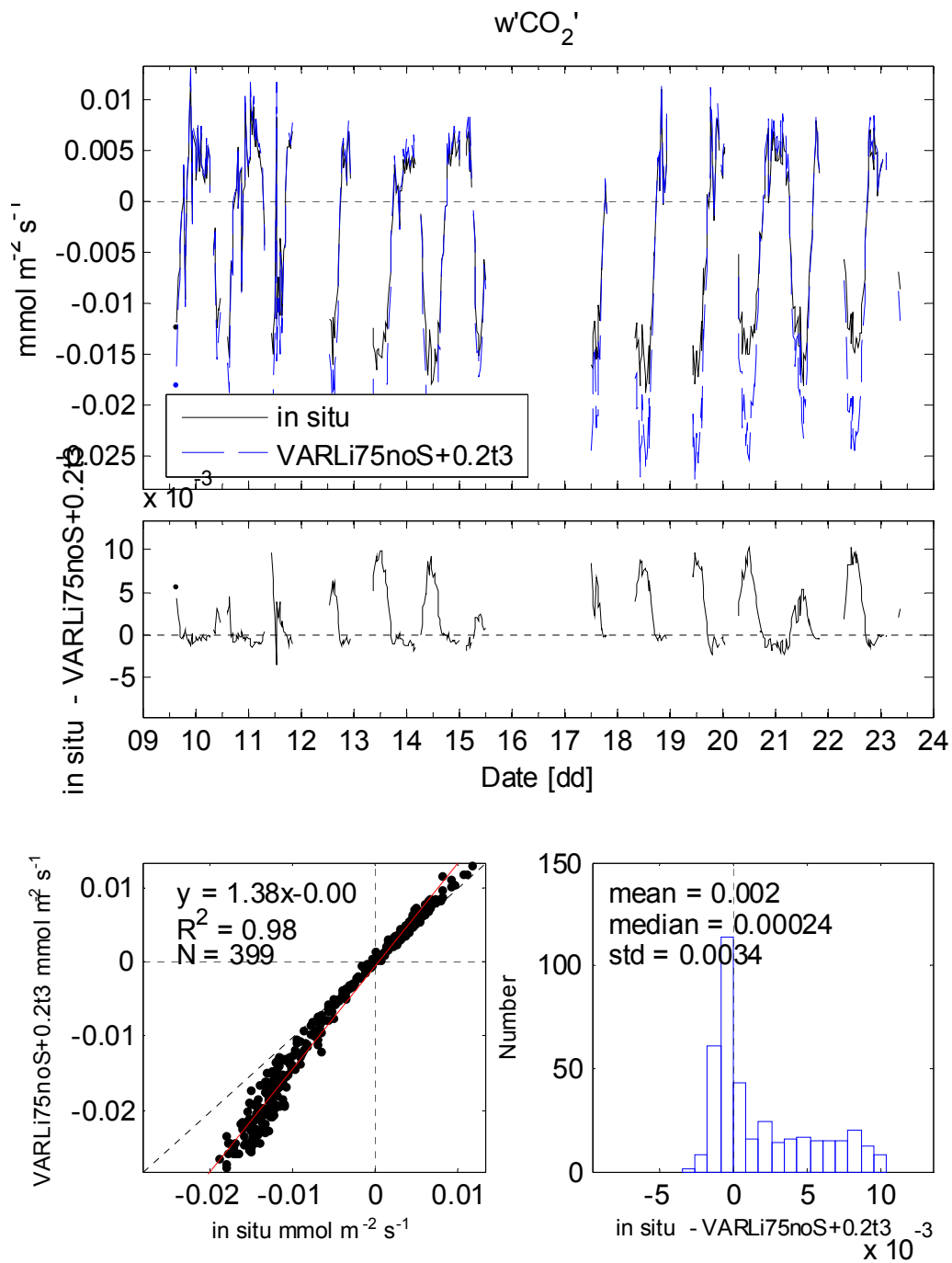


Figure 3 – Covariance between vertical wind and  $CO_2$  measured with the LI-7500 open-path (in situ) and independently processed *in situ* data (VARLi75noS+0.2t3).

Site Name: Vaira Ranch – Ione (US-Var)

Visit Dates: 10 – 24 April 2017

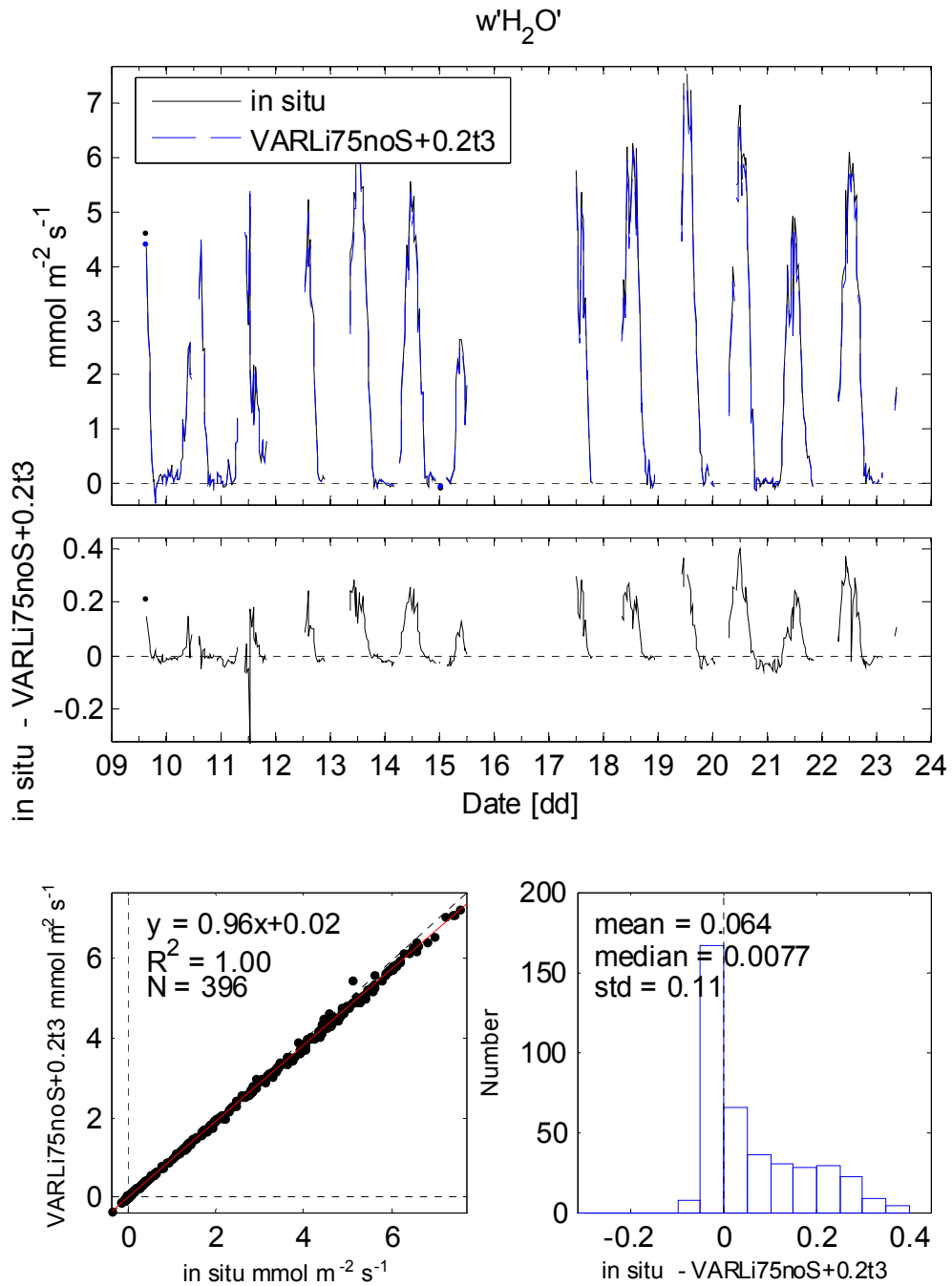


Figure 4 – Covariance between vertical wind and  $H_2O$  measured with the LI-7500 open-path (in situ) and independently processed *in situ* data (VARLi75noS+0.2t3).

Site Name: Vaira Ranch – Ione (US-Var)

Visit Dates: 10 – 24 April 2017

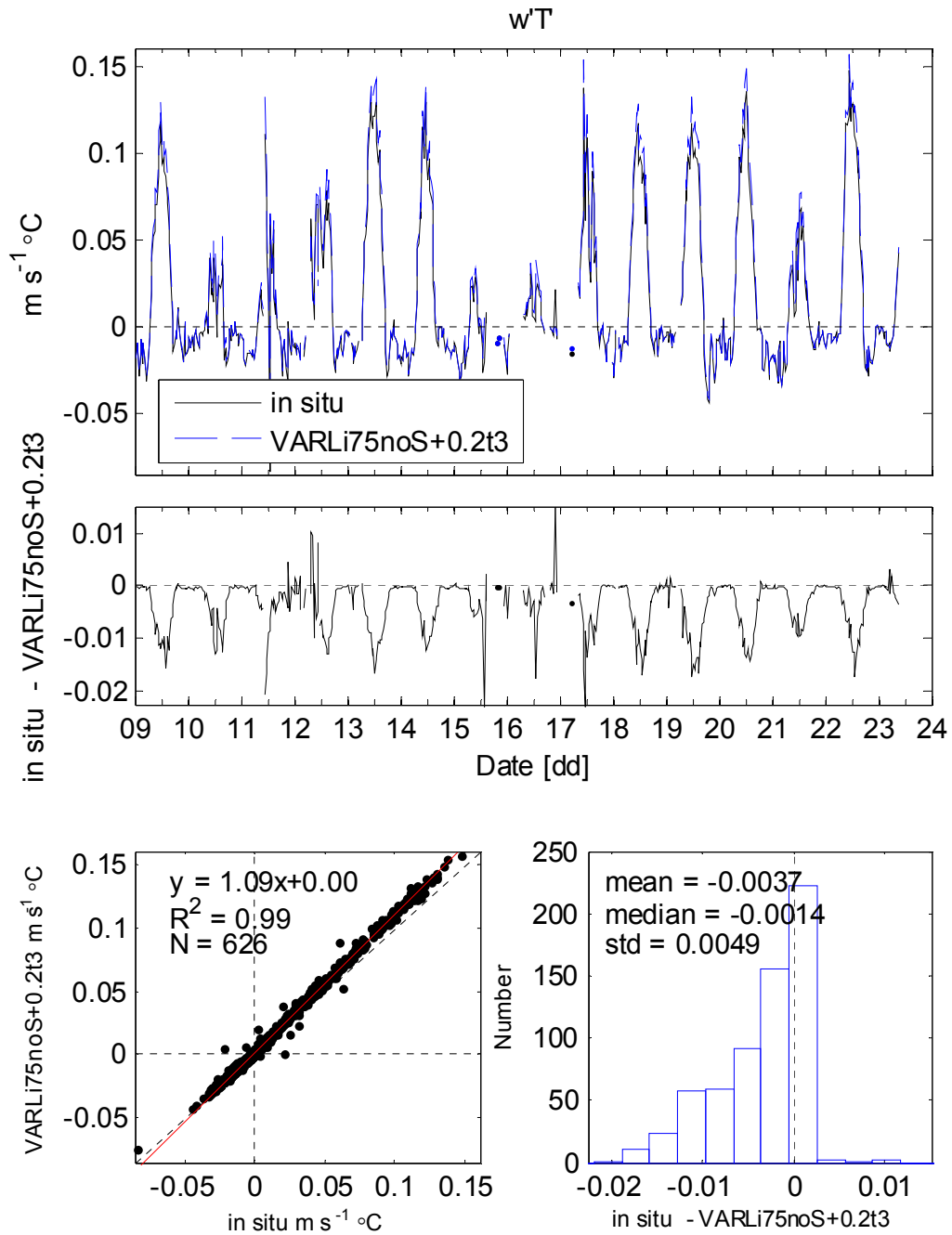


Figure 5 –Covariance between vertical wind and sonic temperature measured with the LI-7500 openpath (in situ) and independently processed *in situ* data (VARLi75noS+0.2t3).

Site Name: Vaira Ranch – Ione (US-Var)  
Visit Dates: 10 – 24 April 2017

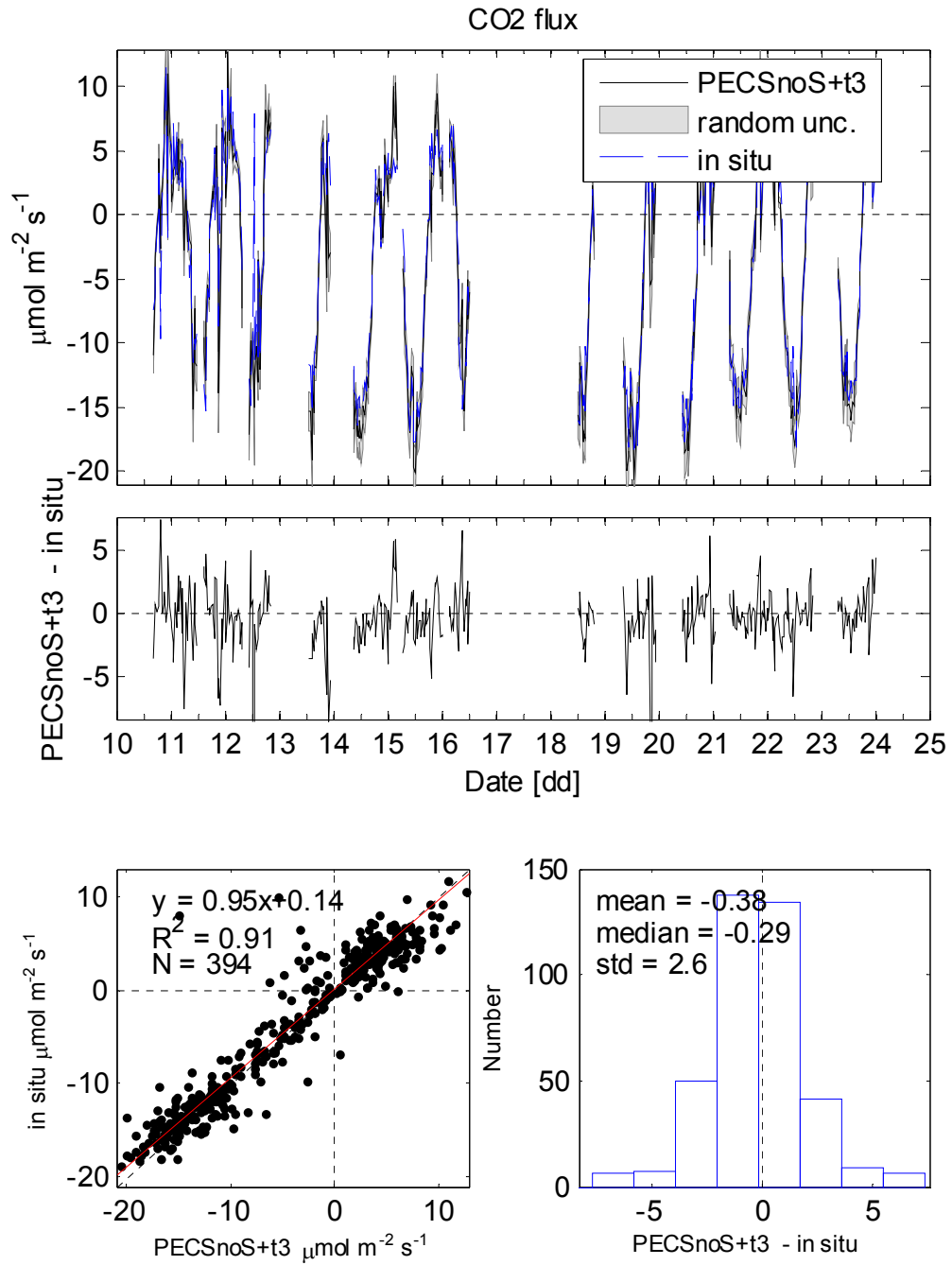


Figure 6 - CO<sub>2</sub> fluxes measured with the LI-7500 open-path (in situ) and LI-7500A (PECS2noS+t3).

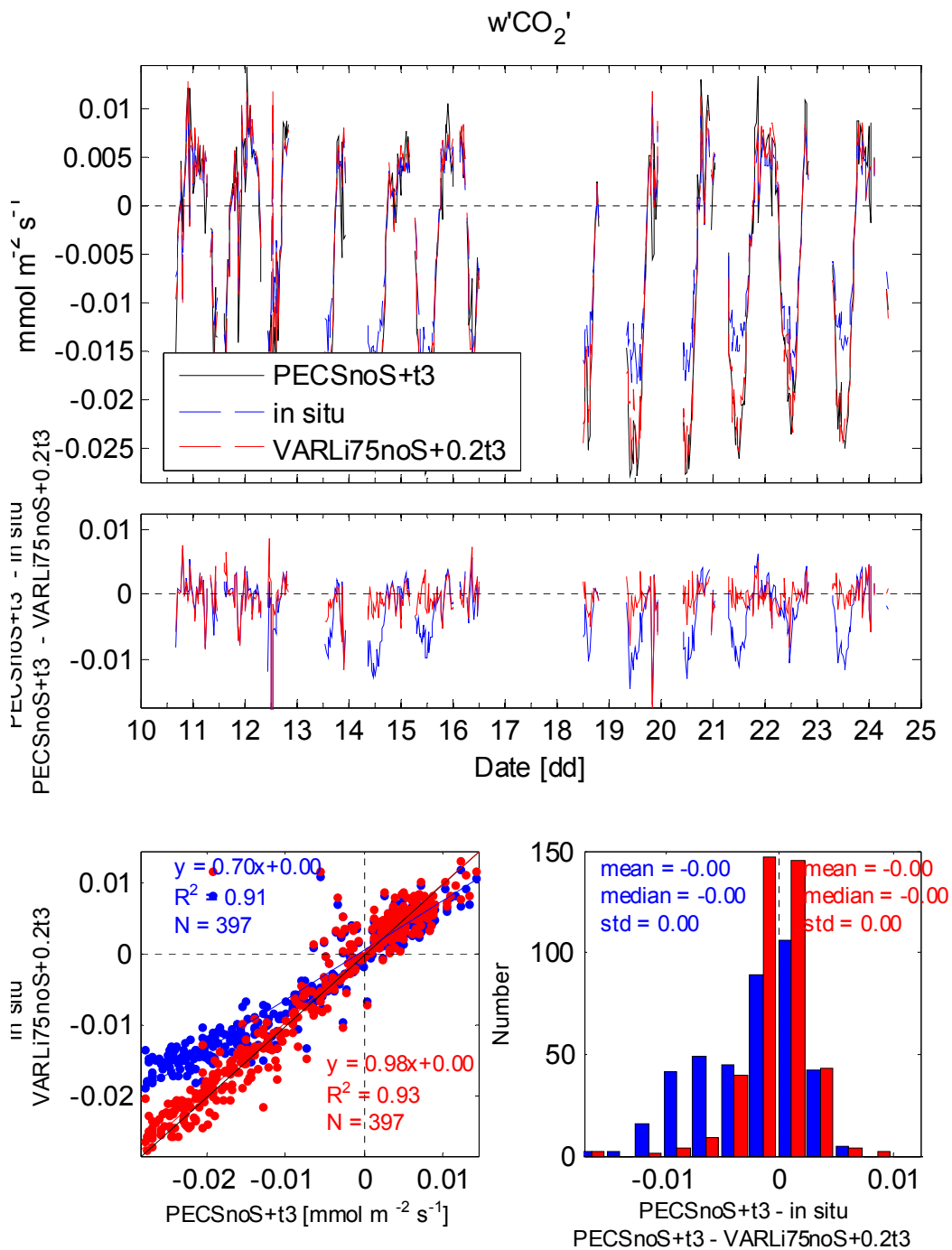


Figure 7 - Covariance of vertical wind and CO<sub>2</sub> measured with the open-path gas analyzers. “PECSnoS+t3” represents PECS2 LI-7500A data and, “in situ”, those provided by site staff while “VARLi75noS+0.2t3” those independently processed data by the AmeriFlux Tech team.

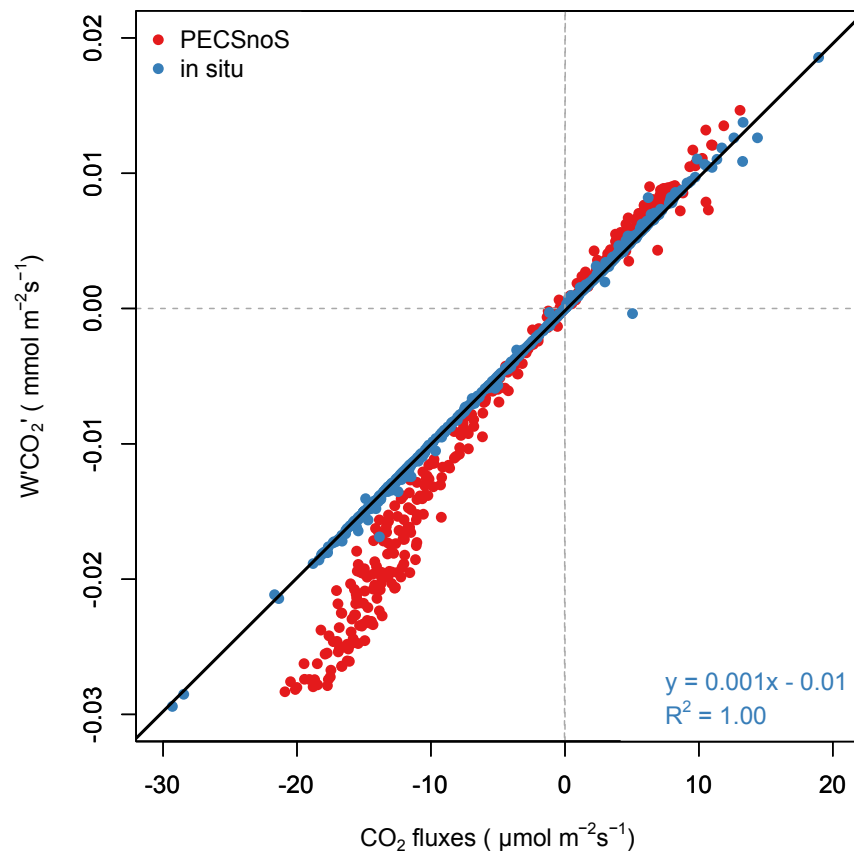


Figure 8 – Comparison between the covariance of vertical wind and CO<sub>2</sub> against final CO<sub>2</sub> fluxes measured with the open-path gas analyzers.

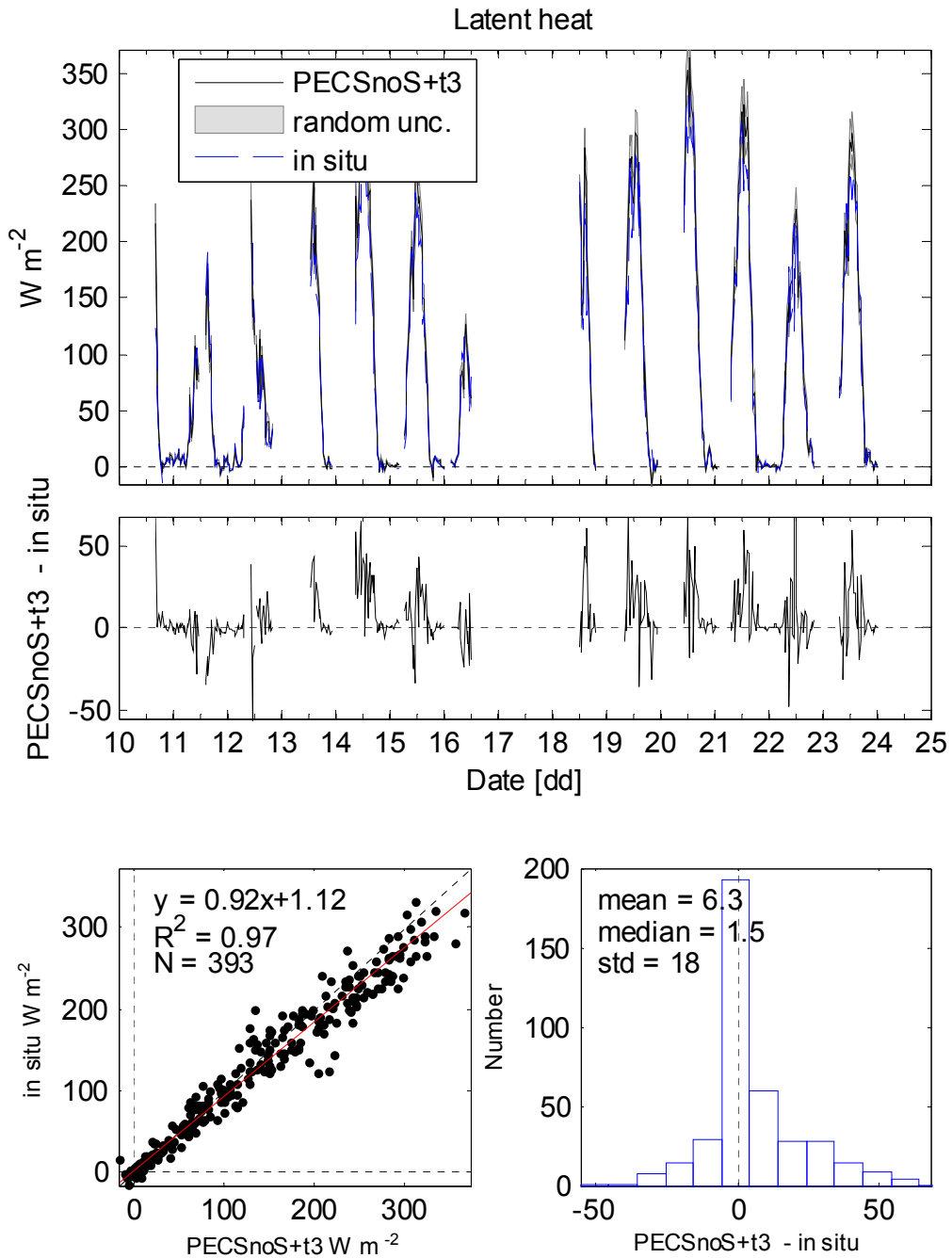


Figure 9 - Latent heat fluxes. “PECSnoS+t3” represents PECS2 data while “in situ” those provided by site staff.

Site Name: Vaira Ranch – Ione (US-Var)

Visit Dates: 10 – 24 April 2017

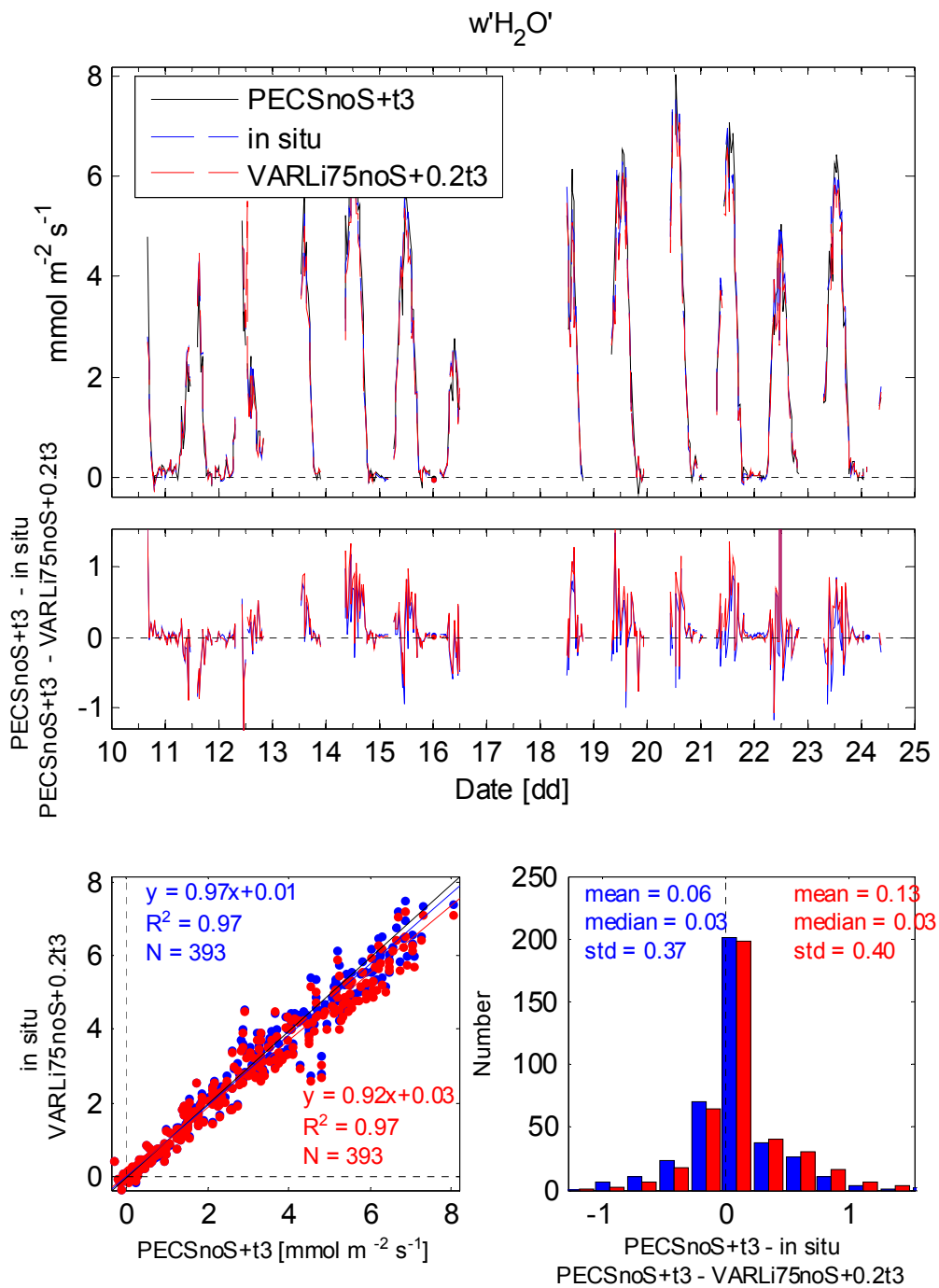


Figure 10 – Covariance of vertical wind and water vapor. “PECSnoS+t3” represents PECS2 data, “in situ” those provided by site staff and “VARLi75noS+0.2t3” those independently processed by the AmeriFlux tech team.

Site Name: Vaira Ranch – Ione (US-Var)

Visit Dates: 10 – 24 April 2017

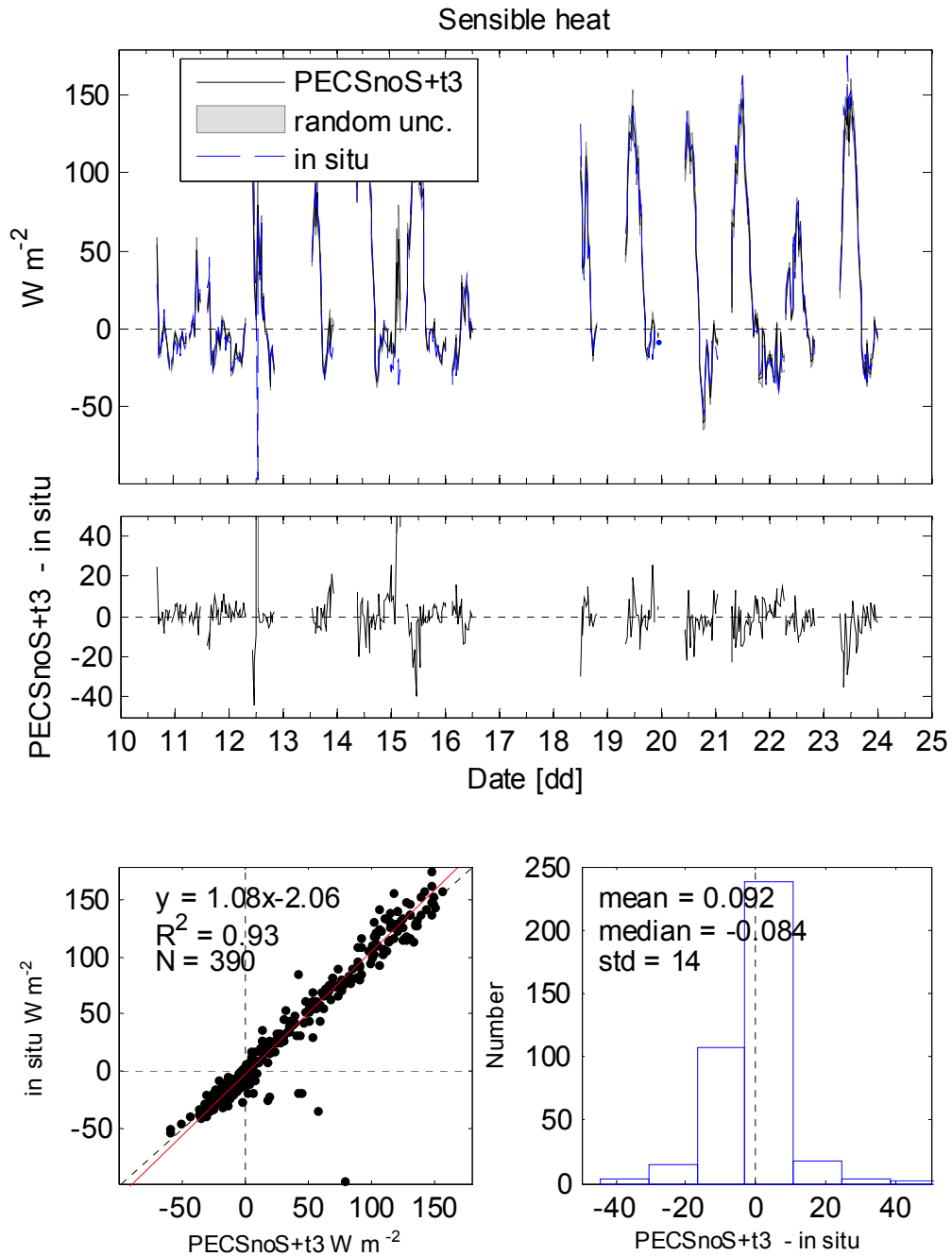


Figure 11 – Sensible heat flux. “PECSnoS+t3” represents PECS2 data while “in situ” those provided by site staff.

Site Name: Vaira Ranch – Ione (US-Var)

Visit Dates: 10 – 24 April 2017

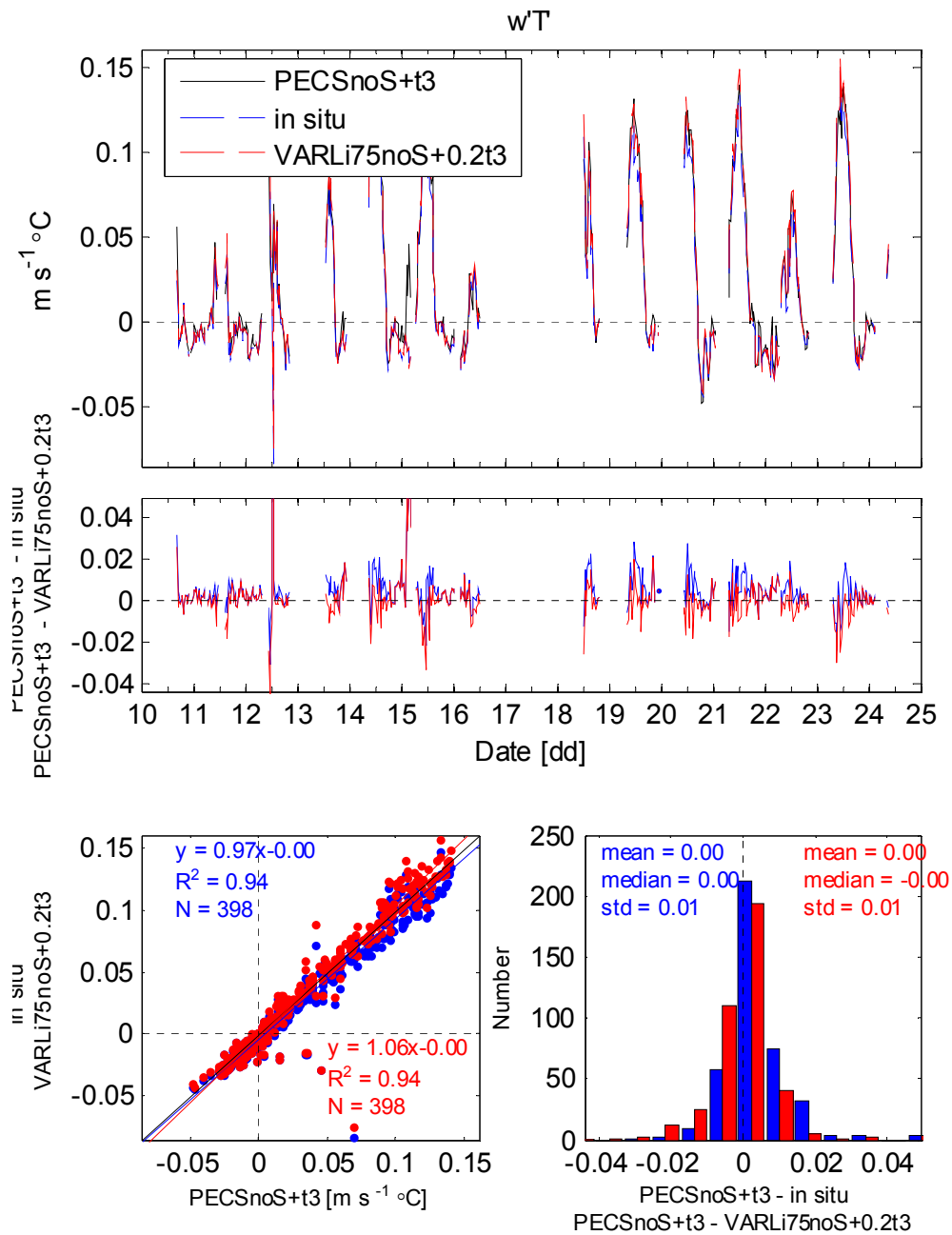


Figure 12 – Covariance of vertical wind and sonic temperature calculated from data recorded with the PECS2 Gill R3-50 and the *in situ* Gill WindMaster. “PECSnoS+t3” represents PECS2 data, “in situ” those provided by site staff and “VARLi75noS+0.2t3” those independently processed by the AmeriFlux tech team.

Site Name: Vaira Ranch – Ione (US-Var)

Visit Dates: 10 – 24 April 2017

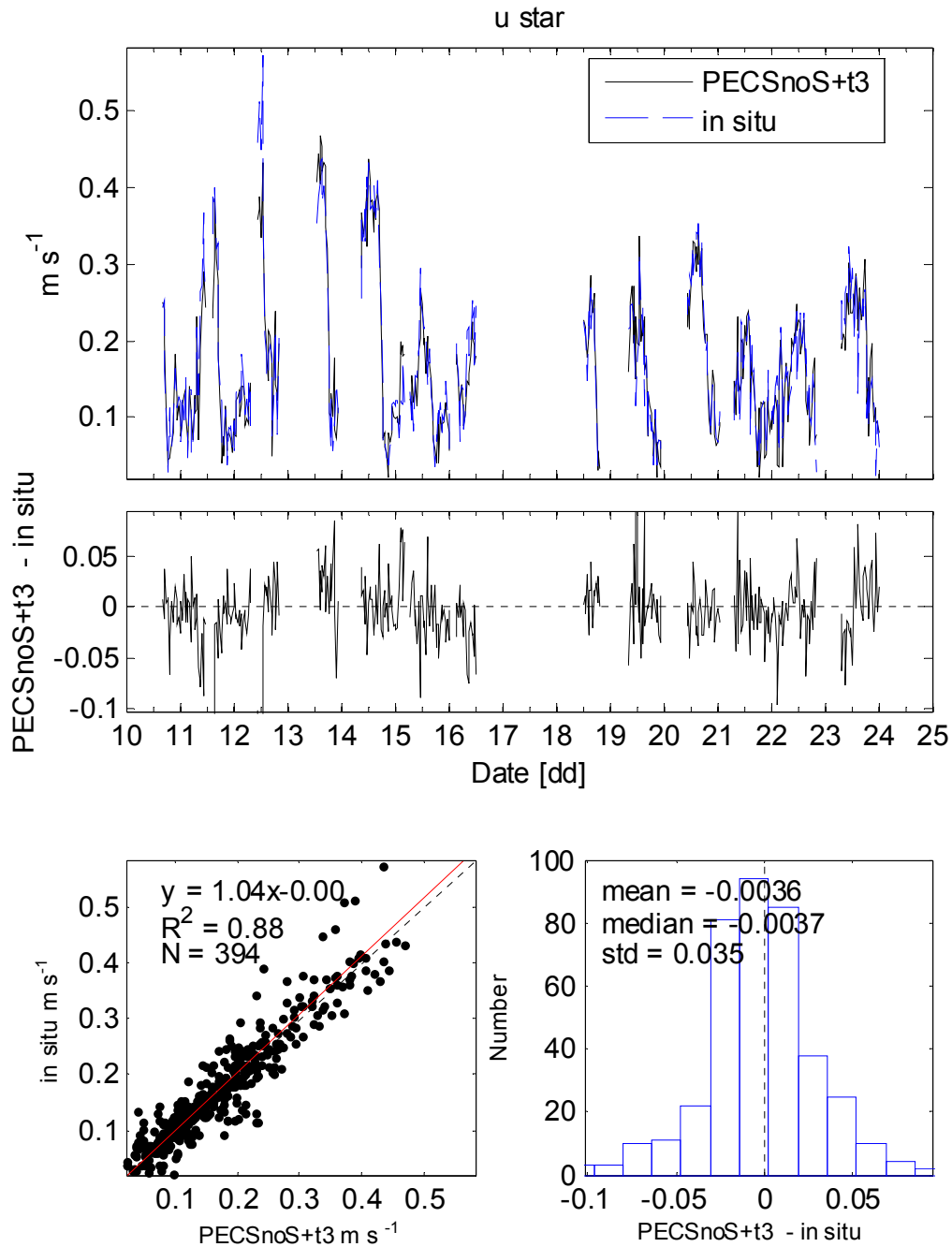


Figure 13 – Friction velocity.

Site Name: Vaira Ranch – Ione (US-Var)  
Visit Dates: 10 – 24 April 2017

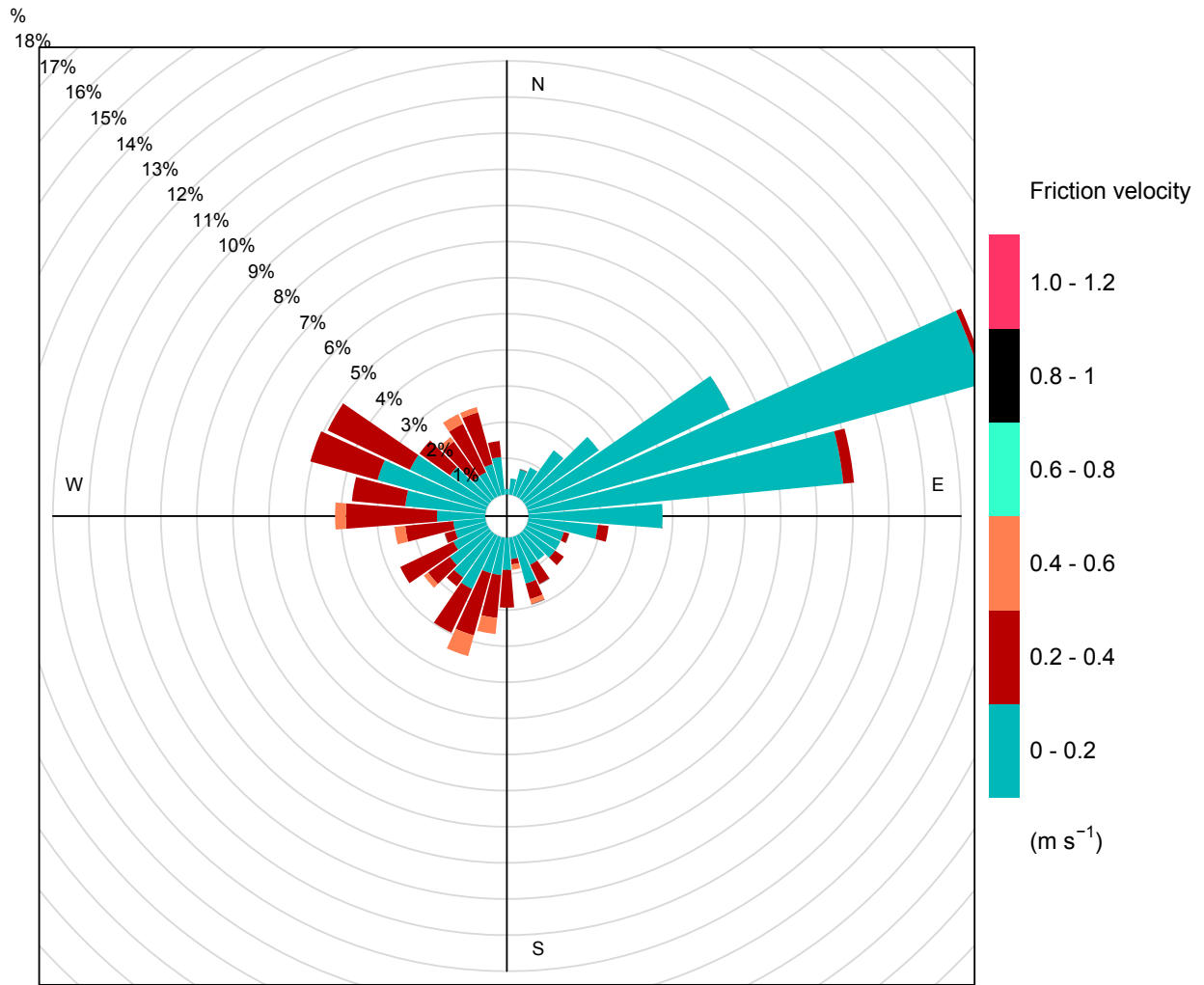


Figure 14 – Friction velocity according to wind direction calculated from *in situ* data.

Site Name: Vaira Ranch – Ione (US-Var)

Visit Dates: 10 – 24 April 2017

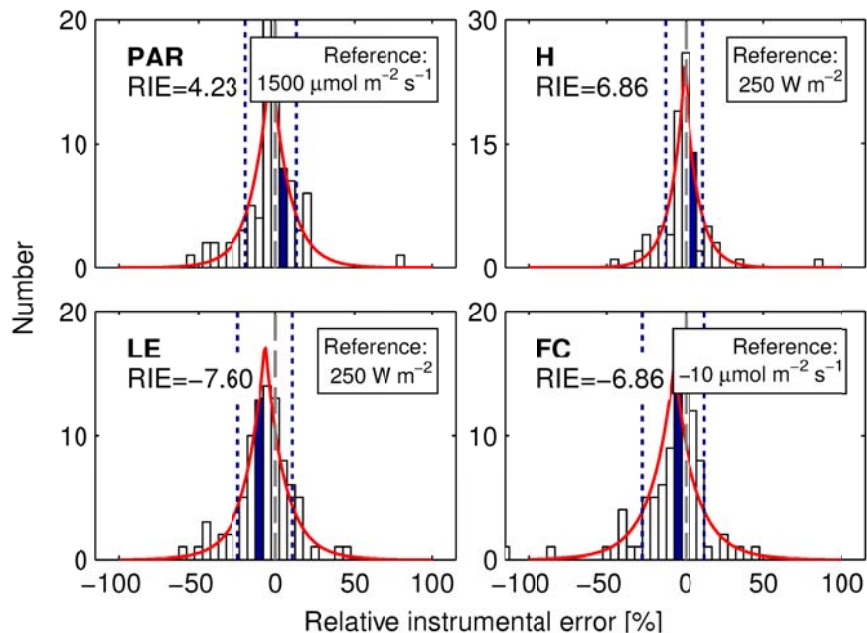


Figure 15 – Histogram of relative instrumental error (RIE) for 4 selected variables based on the accumulated record of AmeriFlux site visits. Colored bar denotes the RIE from this site visit (bar width = 5%). Laplace distribution illustrated in solid red line. Dashed, vertical lines denote mean  $\pm \sqrt{2}\beta$ , where  $\beta$  is a scale parameter describing the Laplace distribution. The term  $\sqrt{2}\beta$  is equivalent to the standard deviation in a normal distribution. Negative RIE values indicate that on average the in situ system has recorded lower values than PECS2 (in this case) and vice versa.

Site Name: Vaira Ranch – Ione (US-Var)  
Visit Dates: 10 – 24 April 2017

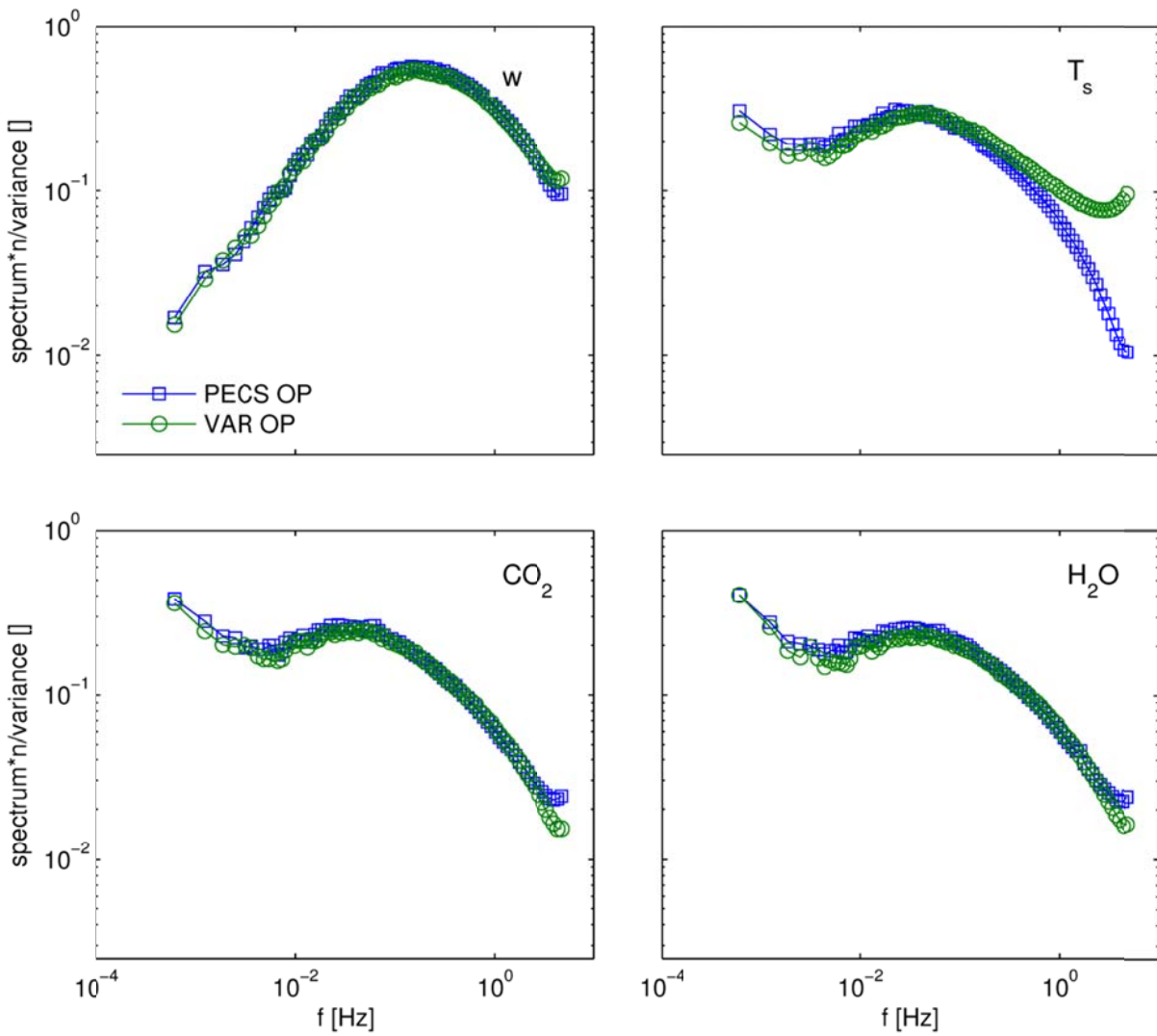


Figure 16 – Ensemble averaged spectra for the open-path systems during dry periods.

Site Name: Vaira Ranch – Ione (US-Var)

Visit Dates: 10 – 24 April 2017

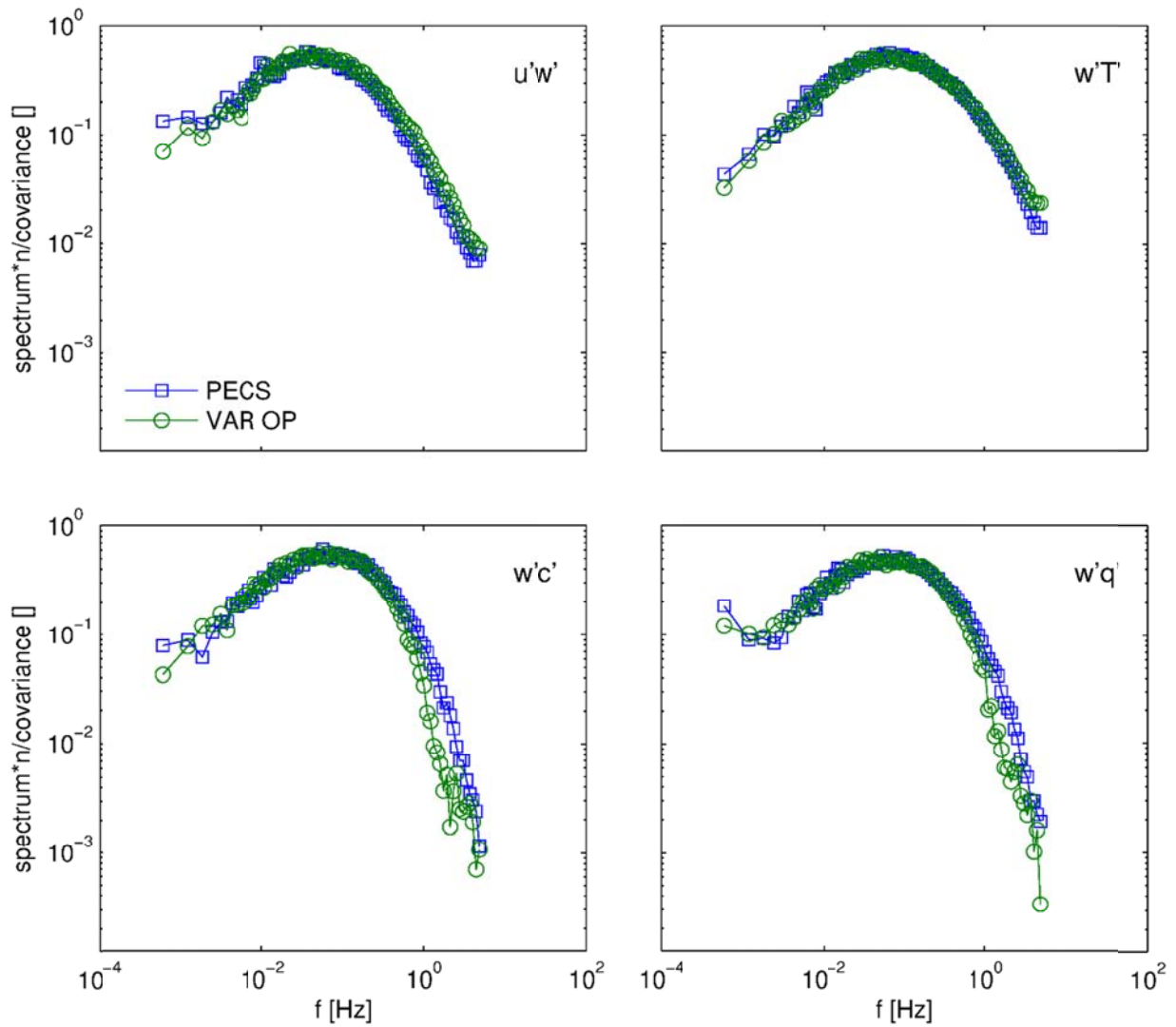


Figure 17 – Ensemble averaged co-spectra for the open-path systems during dry periods.

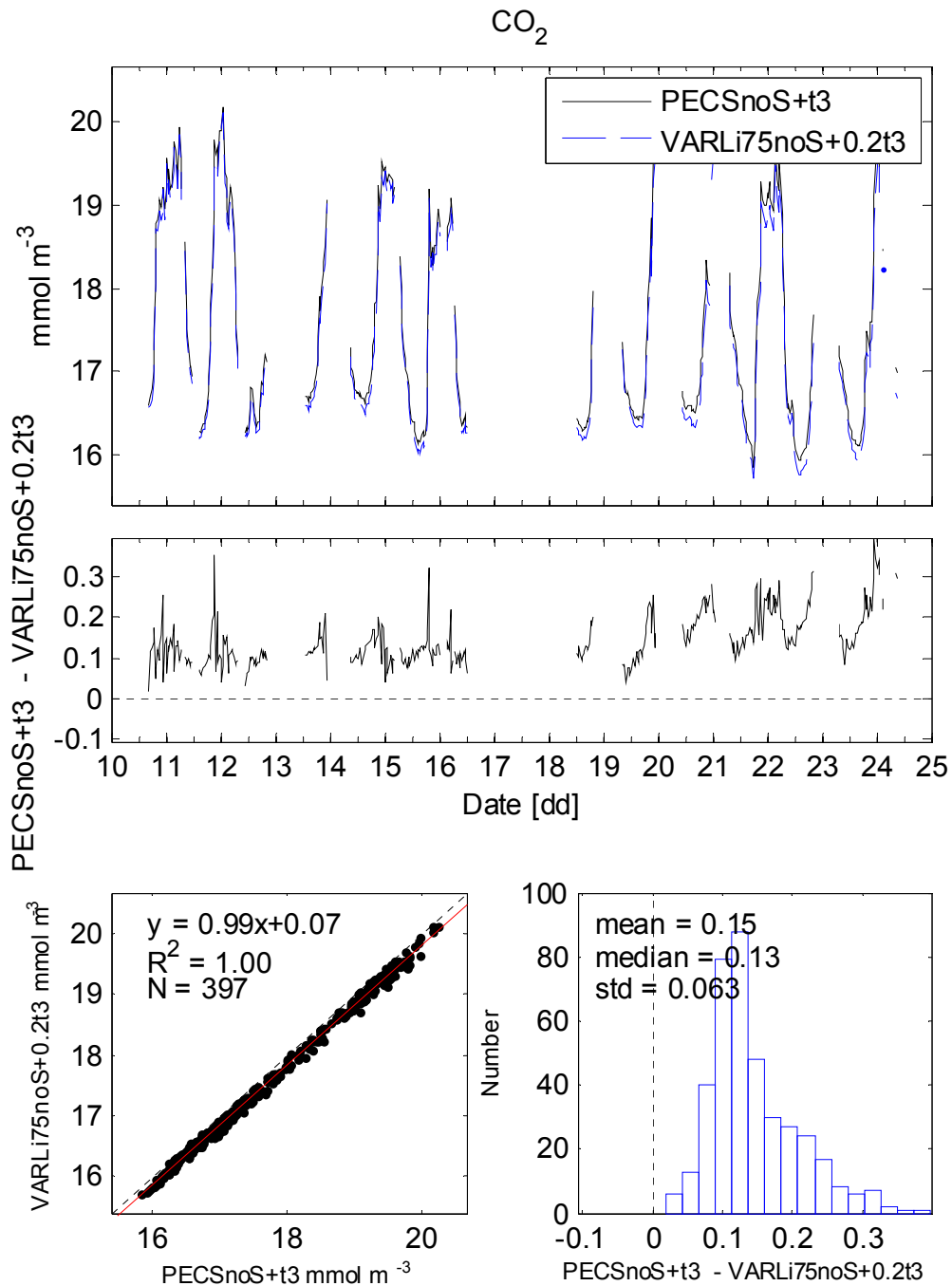


Figure 18 –  $\text{CO}_2$  mole density. . “PECSnoS+t3” represents PECS2 data while “VARLi75noS+0.2t3” those independently processed by the AmeriFlux tech team.

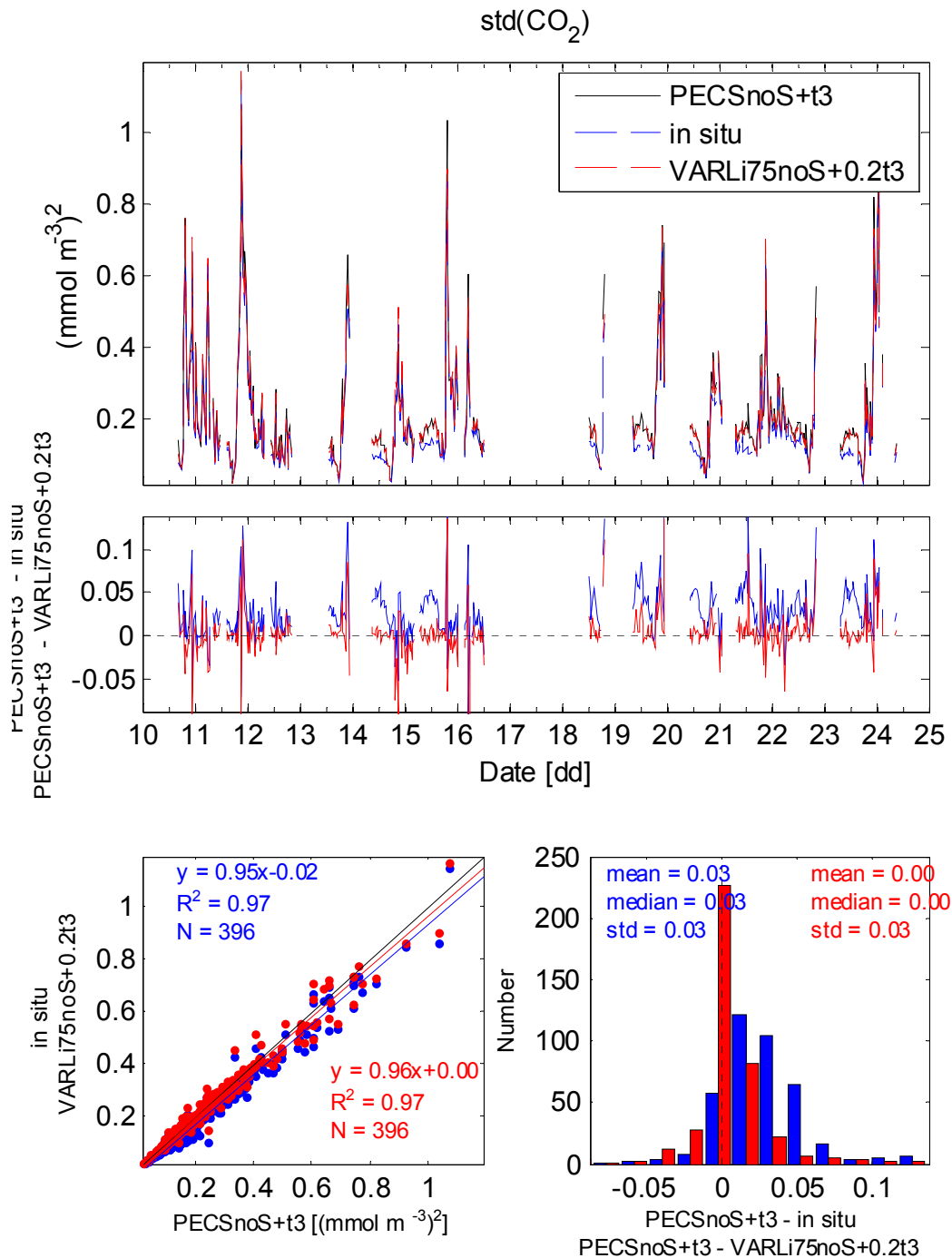


Figure 19 – Standard deviation of CO<sub>2</sub> mole density. “PECSnoS+t3” represents PECS2 data, “in situ” those provided by site staff and “VARLi75noS+0.2t3” those independently processed by the AmeriFlux tech team.

Site Name: Vaira Ranch – Ione (US-Var)

Visit Dates: 10 – 24 April 2017

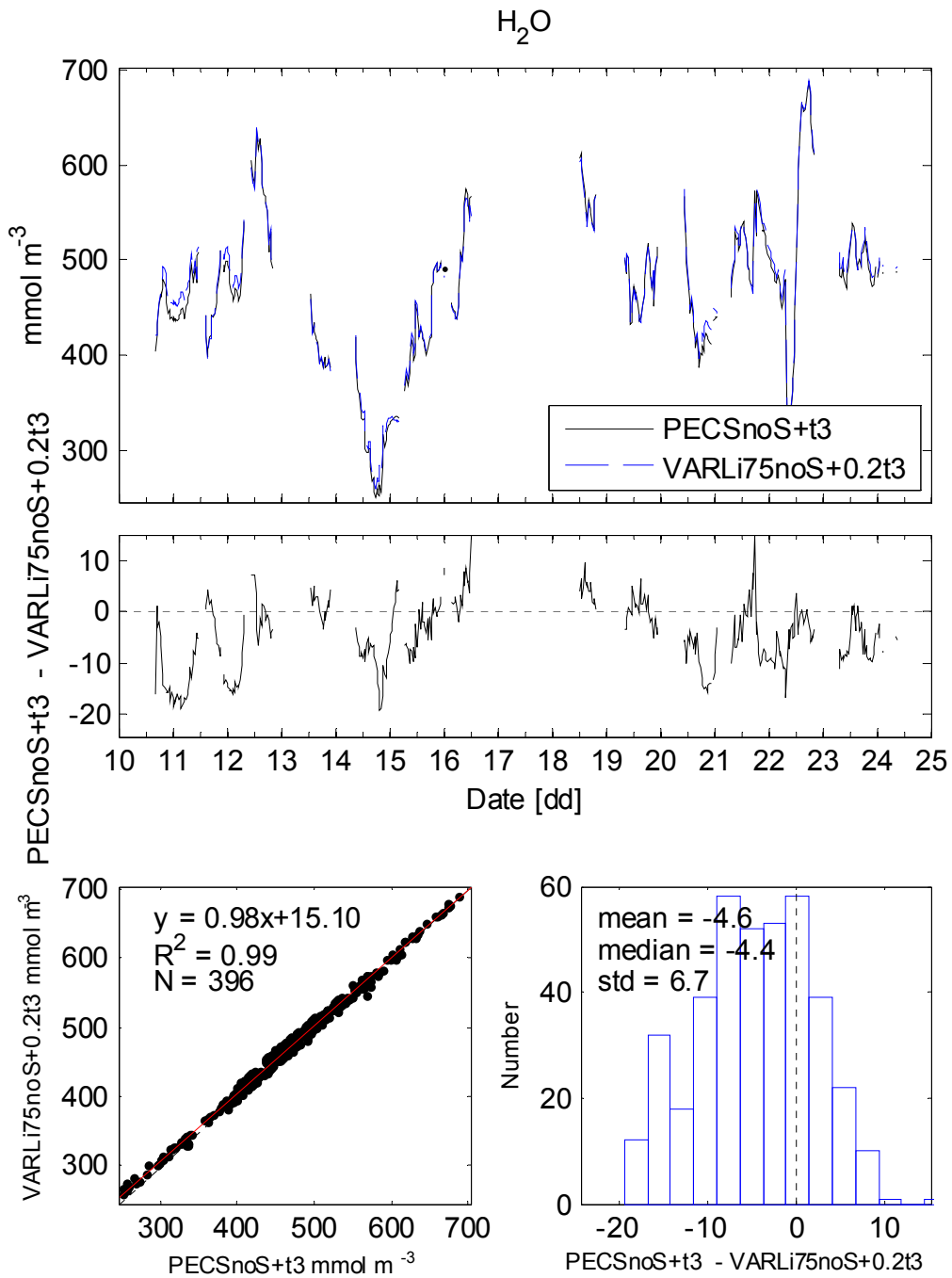


Figure 20 – Water vapor mole density. . “PECSnoS+t3” represents PECS2 data, “in situ” those provided by site staff and “VARLi75noS+0.2t3” those independently processed by the AmeriFlux tech team.

Site Name: Vaira Ranch – Ione (US-Var)

Visit Dates: 10 – 24 April 2017

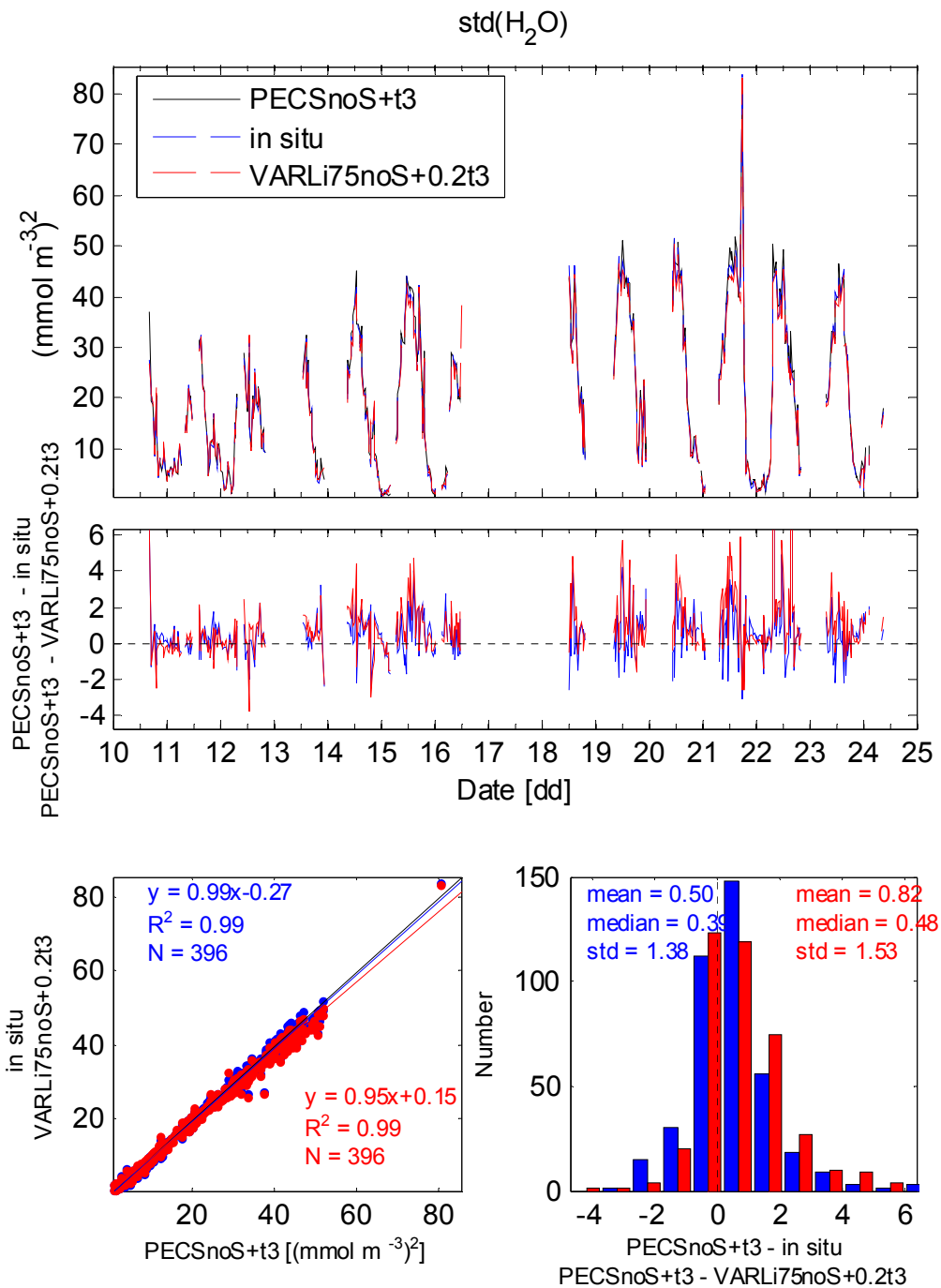


Figure 21 – Standard deviation of water vapor mole density. “PECSnoS+t3” represents PECS2 data, “in situ” those provided by site staff and “VARLi75noS+0.2t3” those independently processed by the AmeriFlux tech team. .

Site Name: Vaira Ranch – Ione (US-Var)

Visit Dates: 10 – 24 April 2017

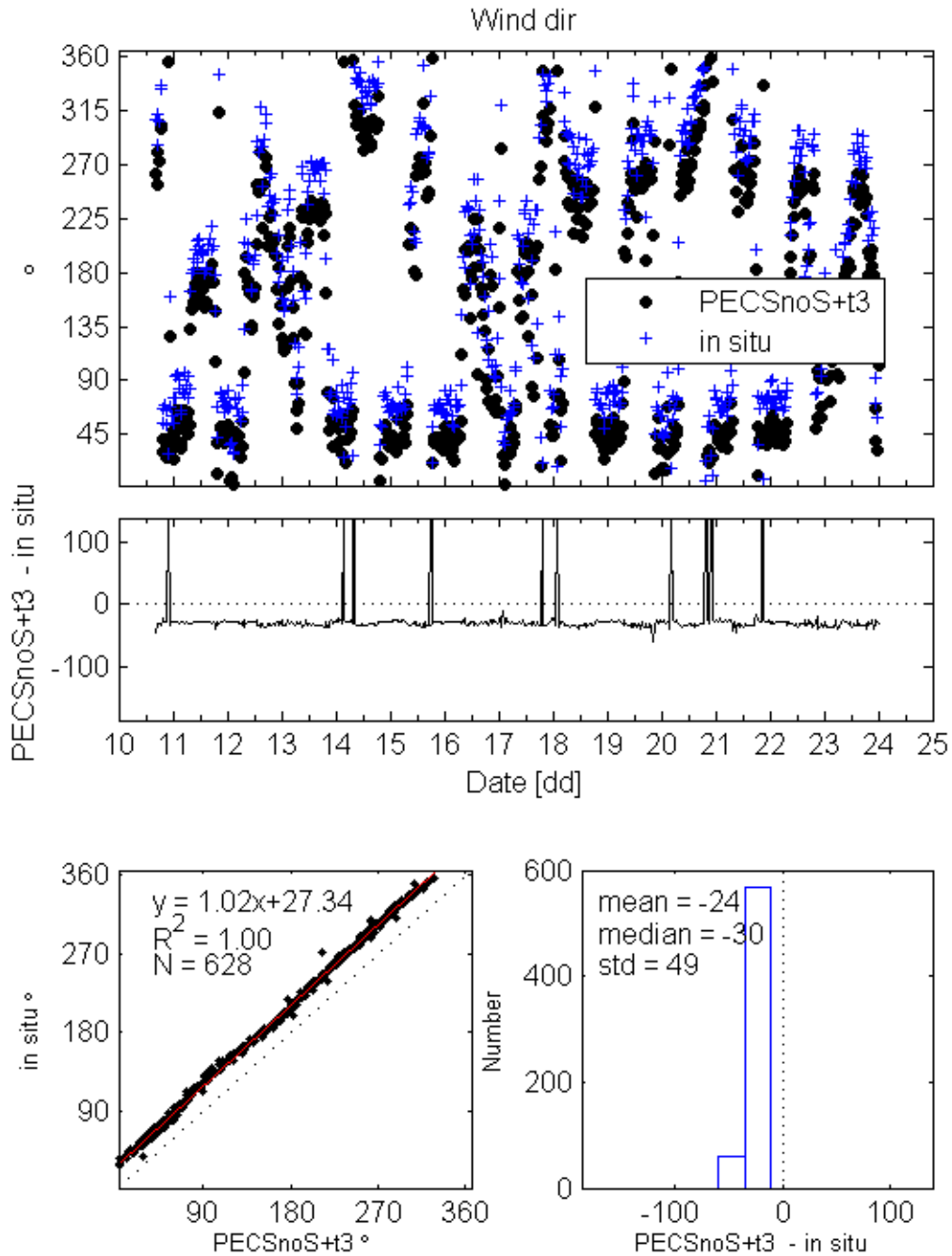


Figure 22 – Wind direction comparison between PECS2 and *in situ* data. The high discrepancy is attributed to the misorientation of the PECS sonic anemometer

Site Name: Vaira Ranch – Ione (US-Var)

Visit Dates: 10 – 24 April 2017

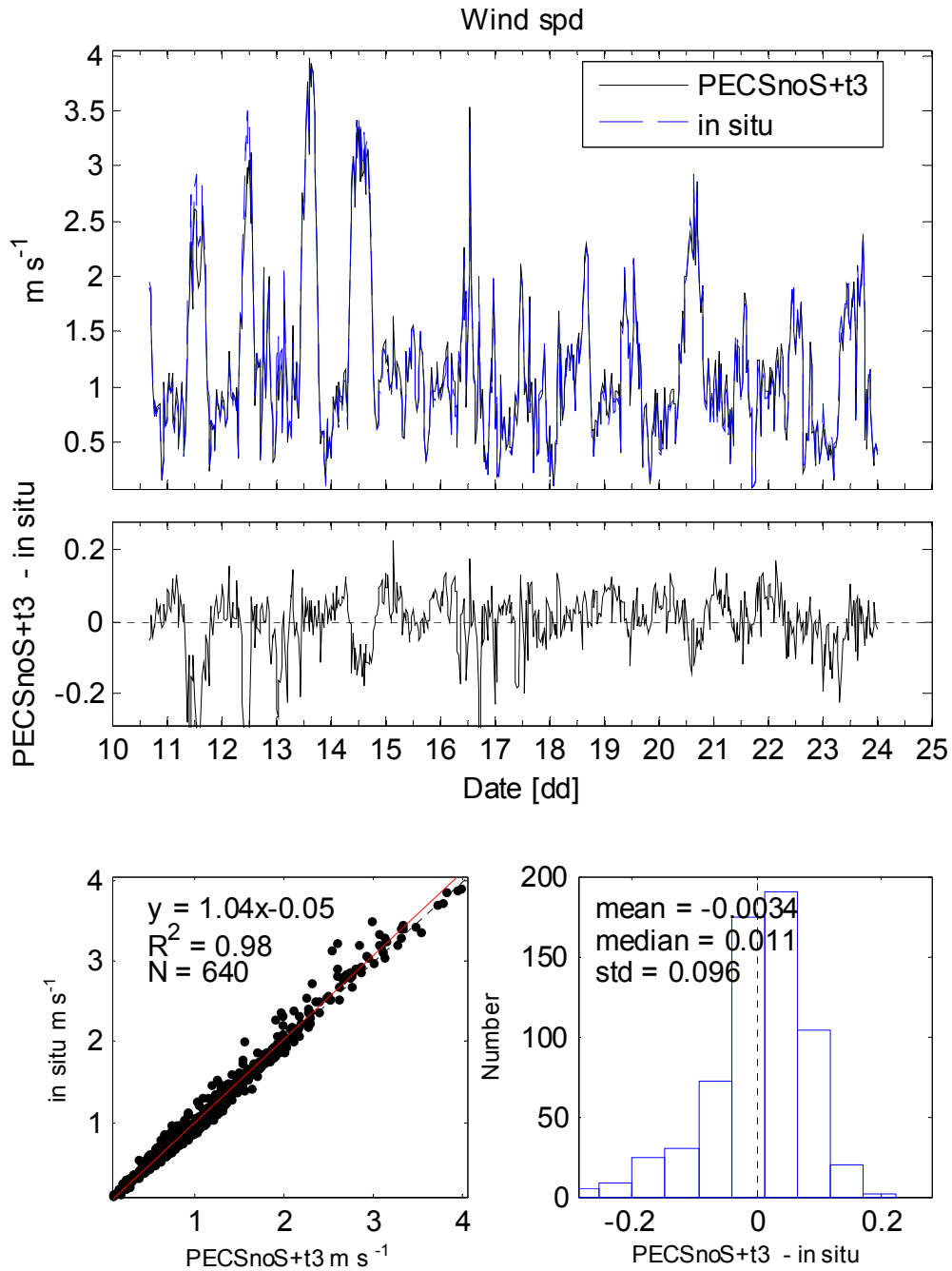


Figure 23 – Wind speed.

Site Name: Vaira Ranch – Ione (US-Var)

Visit Dates: 10 – 24 April 2017

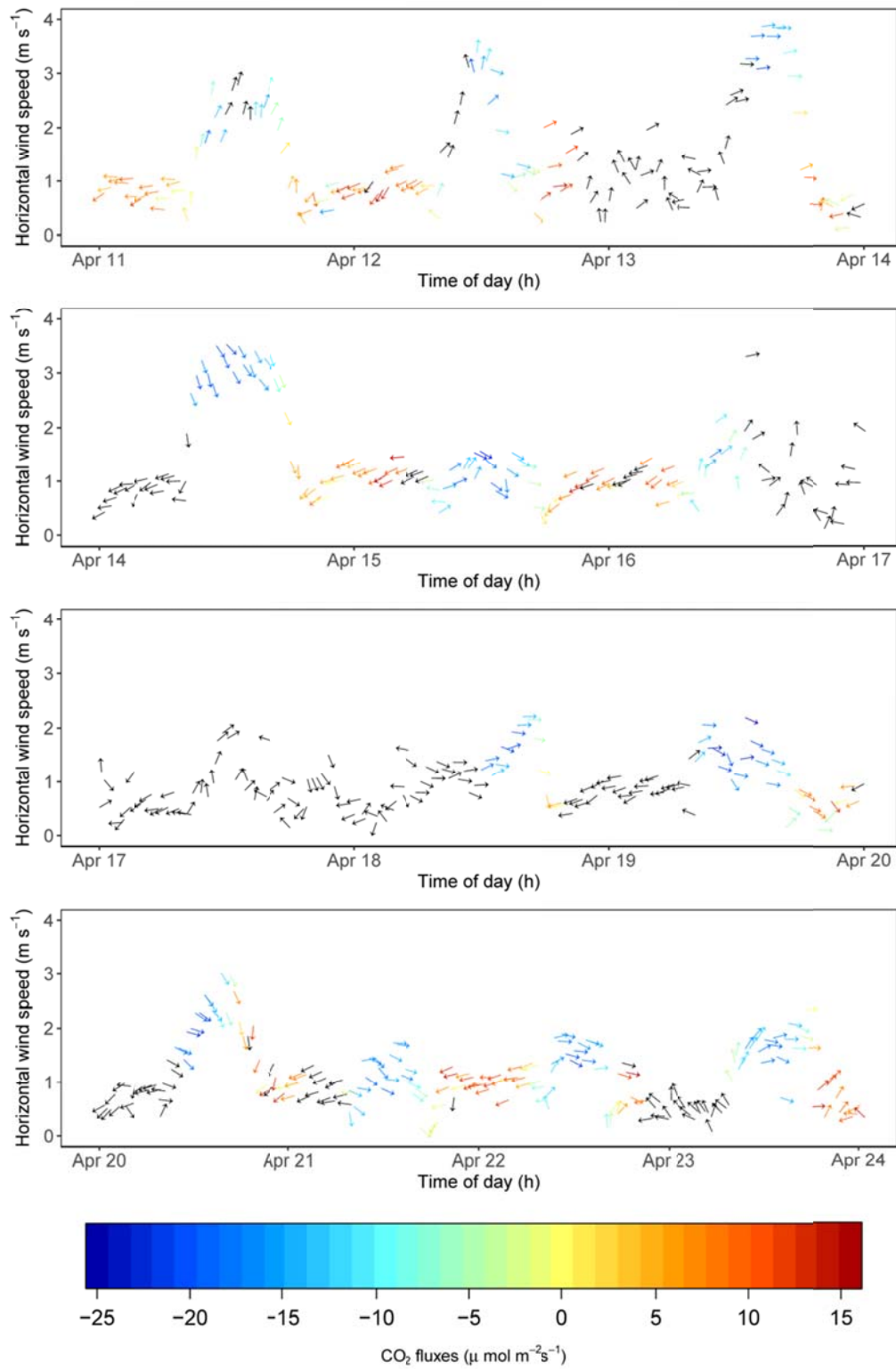


Figure 24 – Wind speed according to wind direction (represented by directional arrows) for the site visit duration (full days only), estimated from *in situ* data. Black arrows represent missing CO<sub>2</sub> flux values.

Site Name: Vaira Ranch – Ione (US-Var)  
Visit Dates: 10 – 24 April 2017

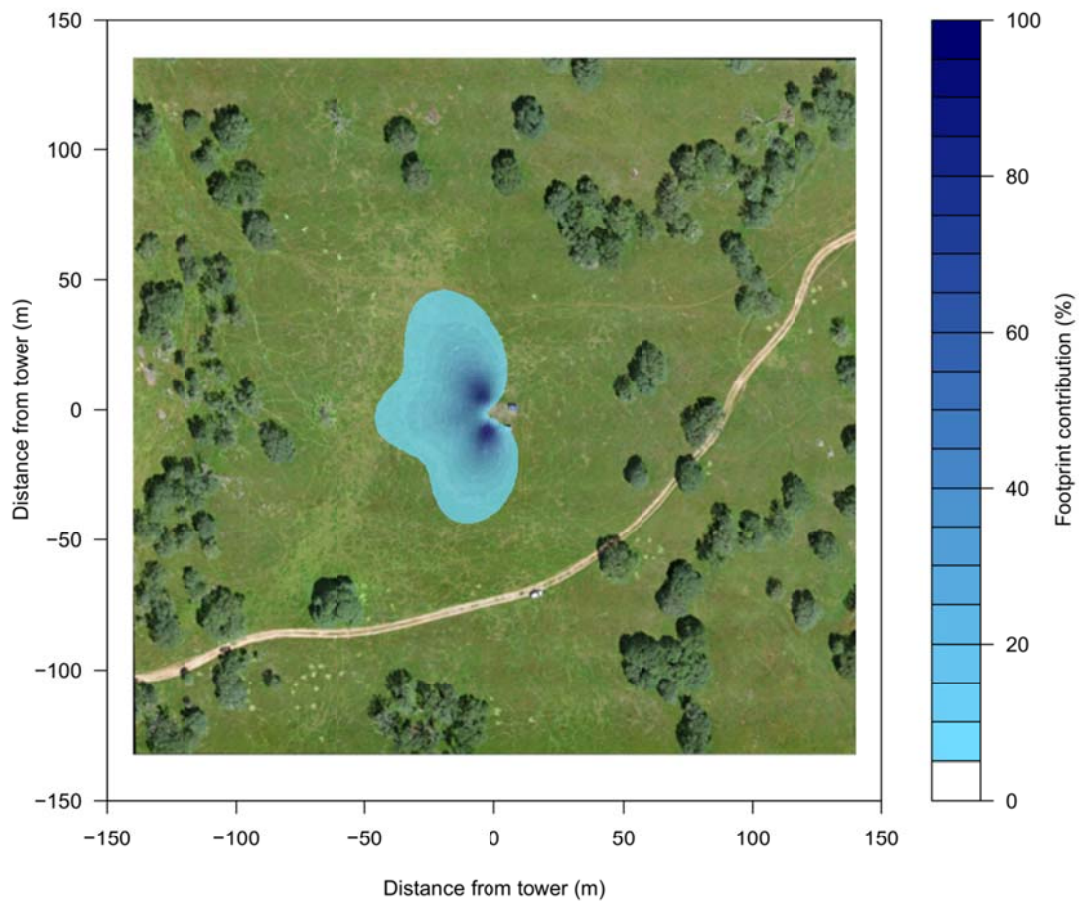


Figure 25 – Averaged footprint distribution (Kormann & Meixner, 2001) for the entire site visit measurement period, excluding periods with low turbulence values ( $u^* < 0.2$ ).

Site Name: Vaira Ranch – Ione (US-Var)

Visit Dates: 10 – 24 April 2017

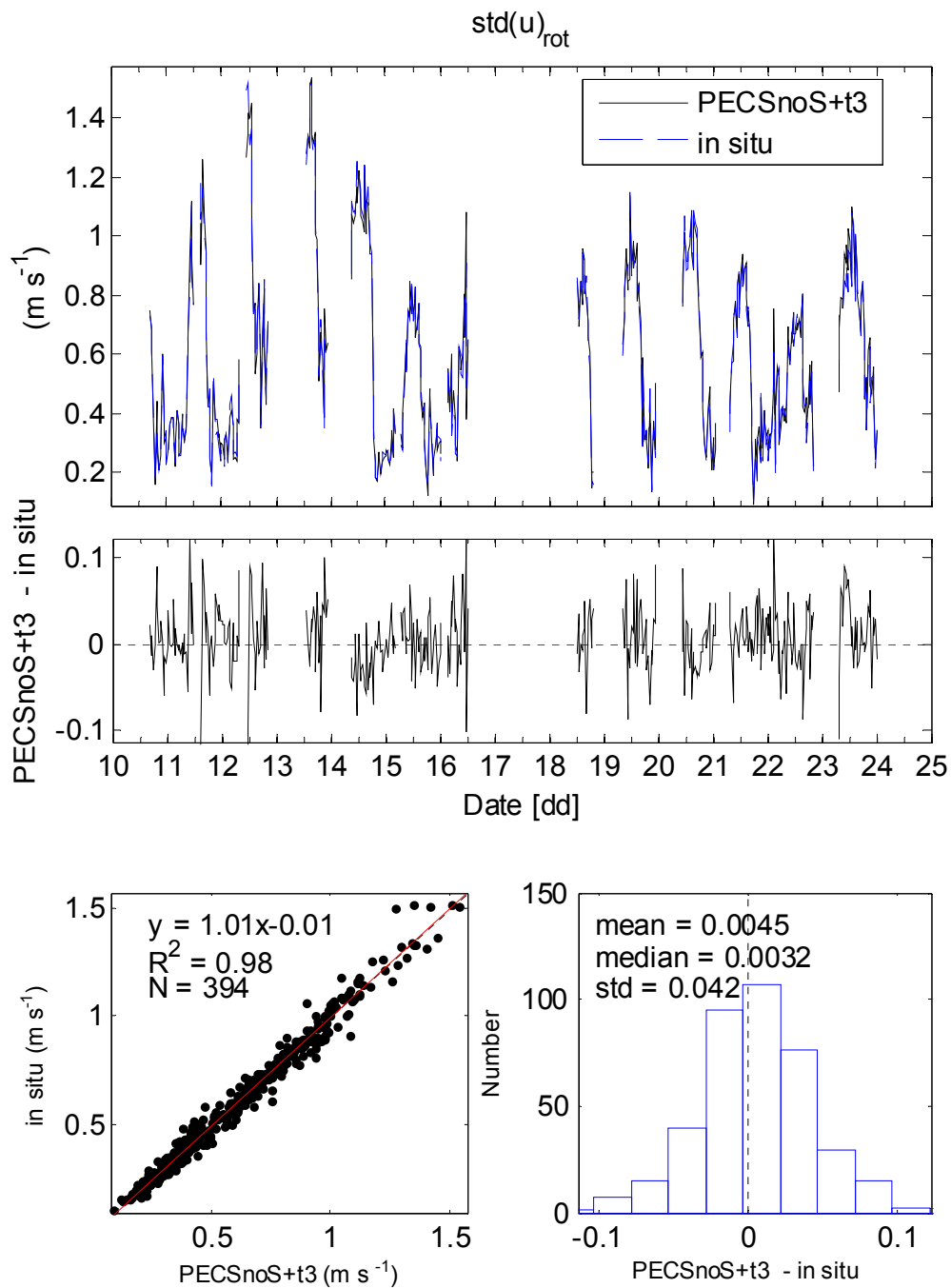


Figure 26 – Standard deviation of the rotated u-wind component.

Site Name: Vaira Ranch – Ione (US-Var)

Visit Dates: 10 – 24 April 2017

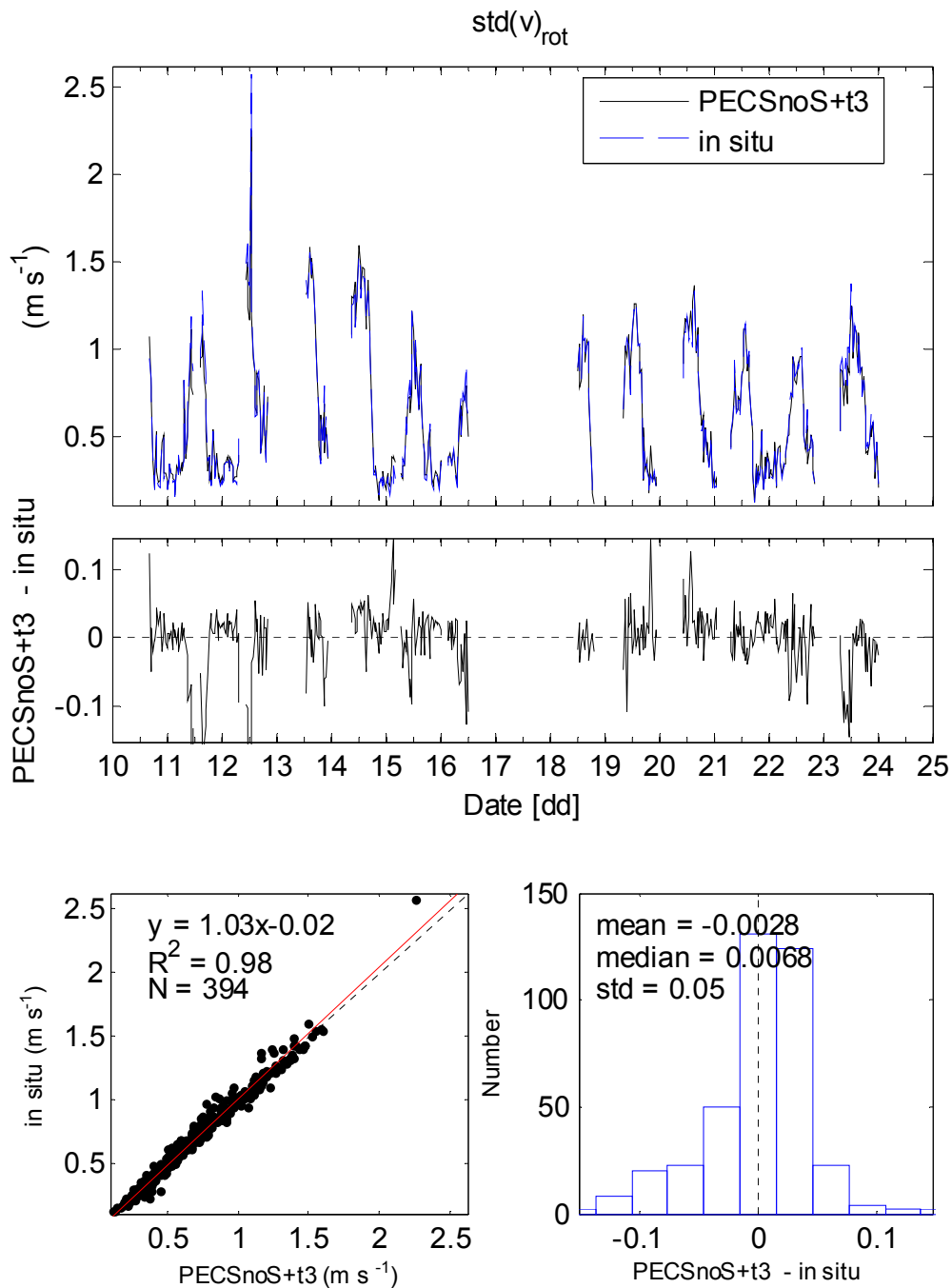


Figure 27 – Standard deviation of the rotated v-wind component.

Site Name: Vaira Ranch – Ione (US-Var)  
Visit Dates: 10 – 24 April 2017

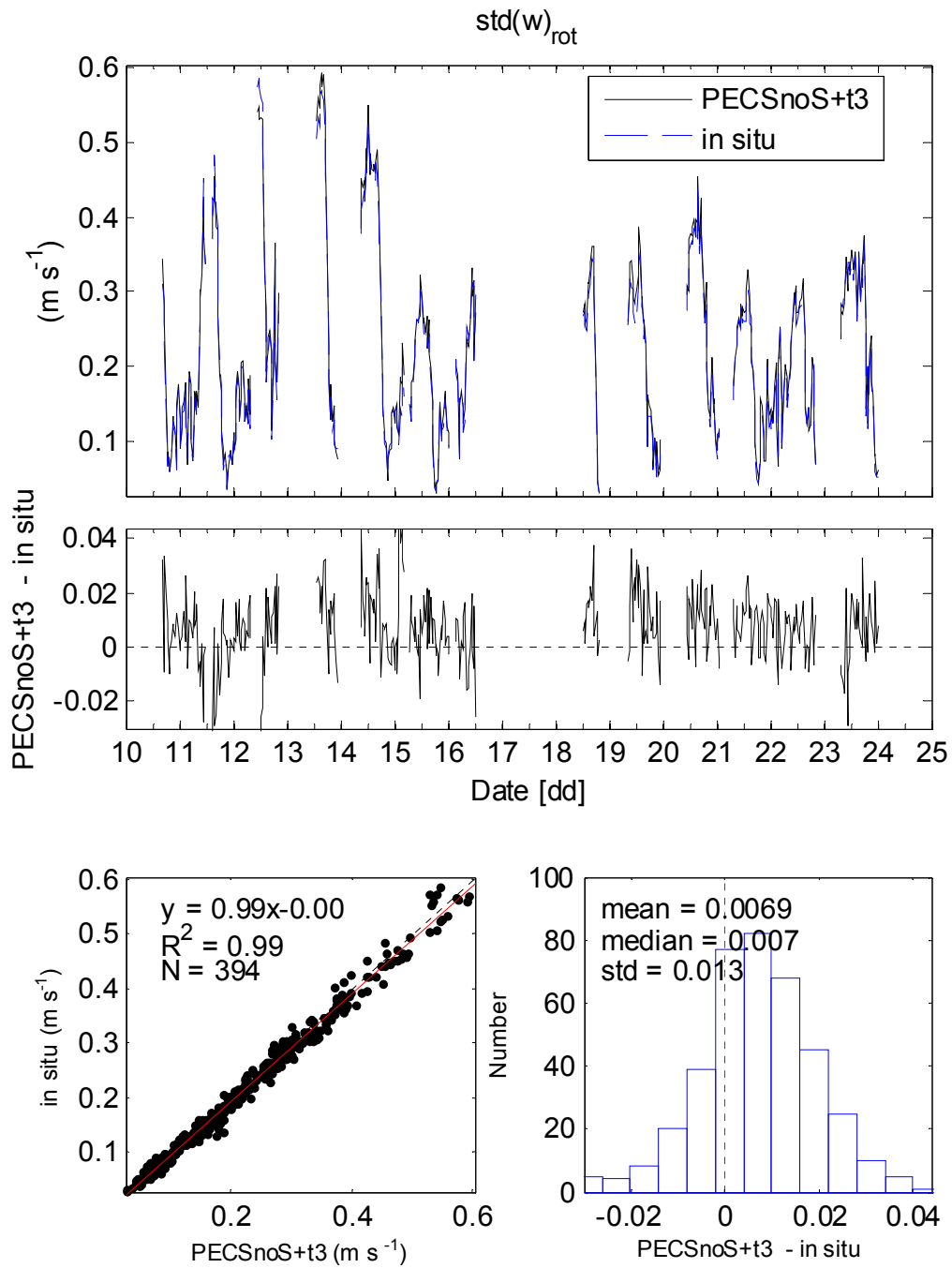


Figure 28 – Standard deviation of the rotated w-wind component.

Site Name: Vaira Ranch – Ione (US-Var)

Visit Dates: 10 – 24 April 2017

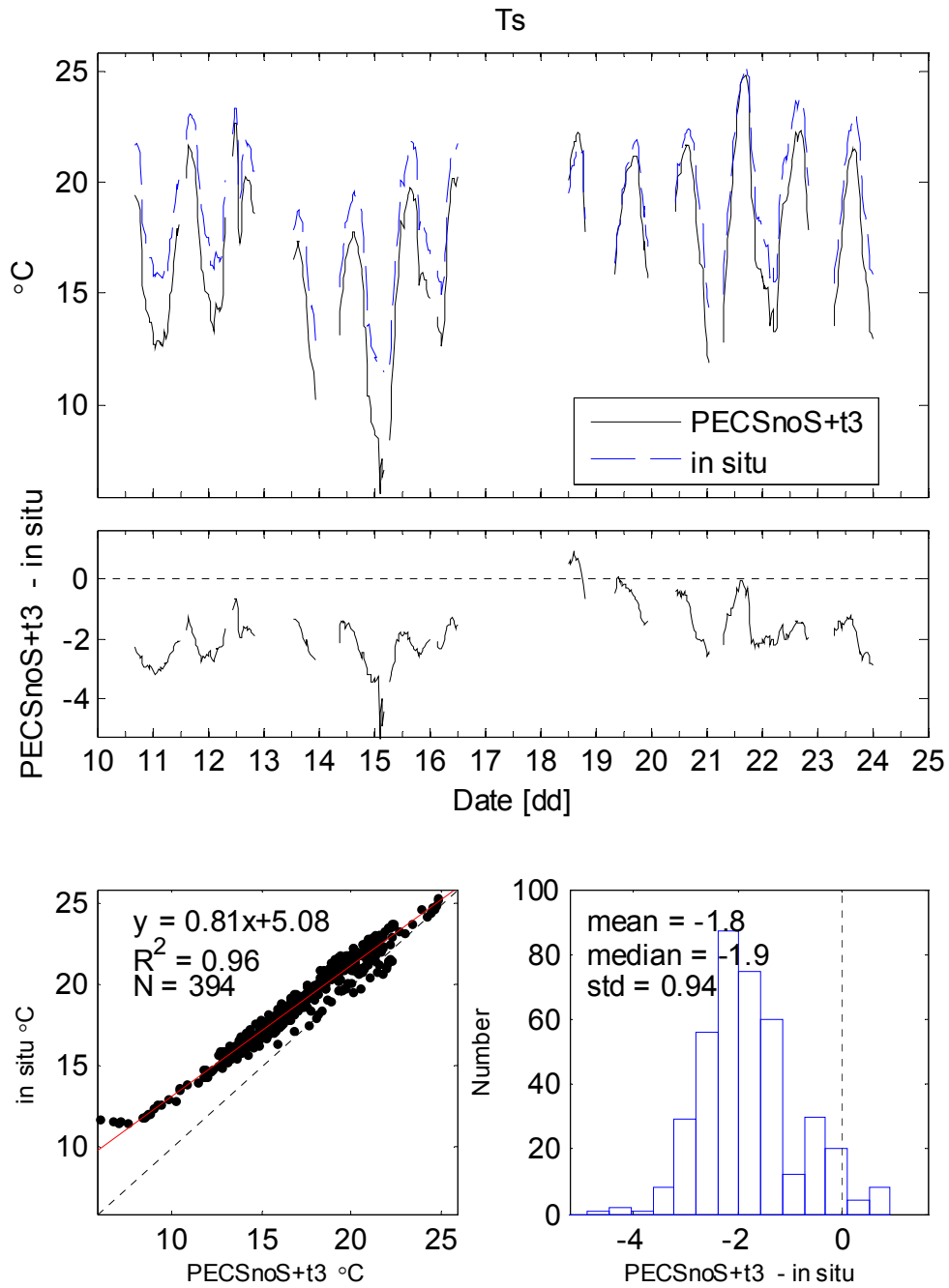


Figure 29 – Mean sonic temperature.

Site Name: Vaira Ranch – Ione (US-Var)

Visit Dates: 10 – 24 April 2017

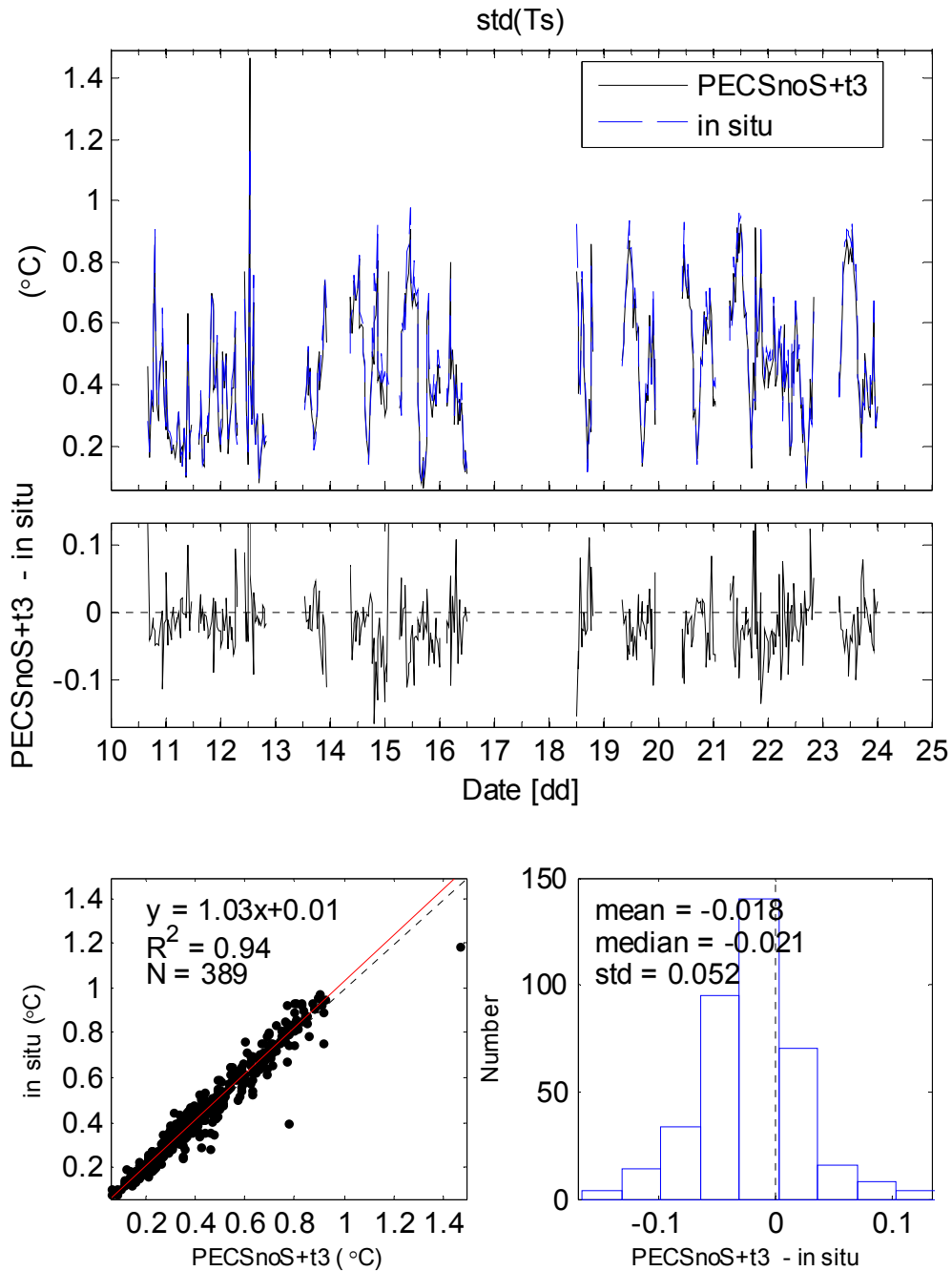


Figure 30 – Standard deviation of the sonic temperature distribution.

Site Name: Vaira Ranch – Ione (US-Var)

Visit Dates: 10 – 24 April 2017

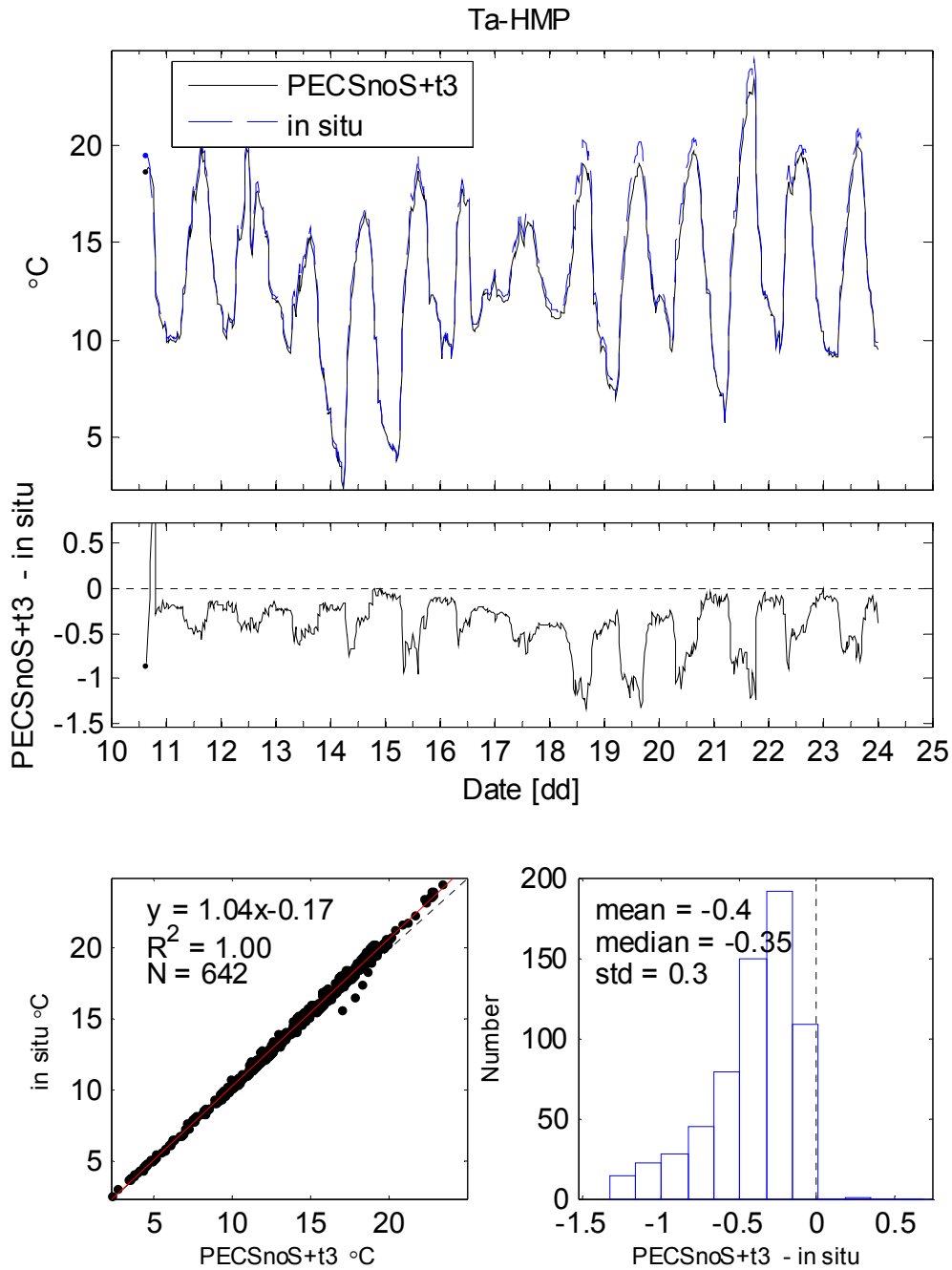


Figure 31 – Ambient air temperature measured with the PECS2 HMP155 and the *in situ* HMP45 temperature and relative humidity probes.

Site Name: Vaira Ranch – Ione (US-Var)

Visit Dates: 10 – 24 April 2017

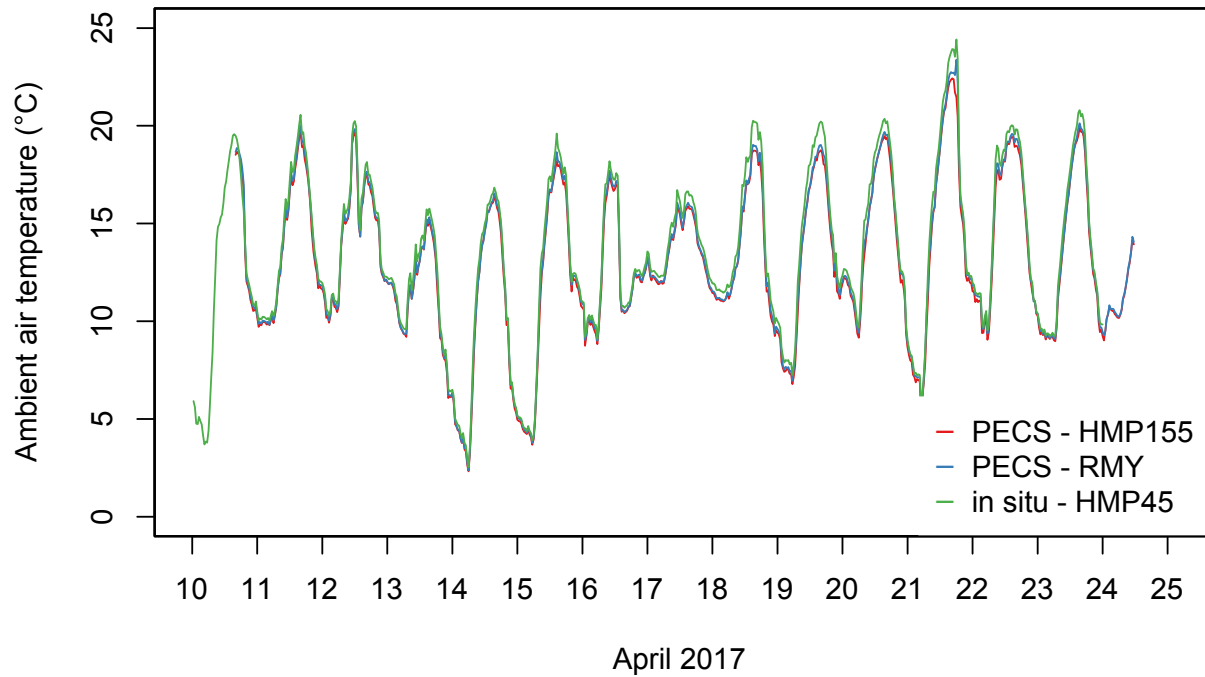


Figure 32 – Ambient air temperature measured with the PECS2 HMP155 and the *in situ* HMP45 temperature and relative humidity probes together with the PECS2 RM Young aspirated temperature probe.

Site Name: Vaira Ranch – Ione (US-Var)

Visit Dates: 10 – 24 April 2017

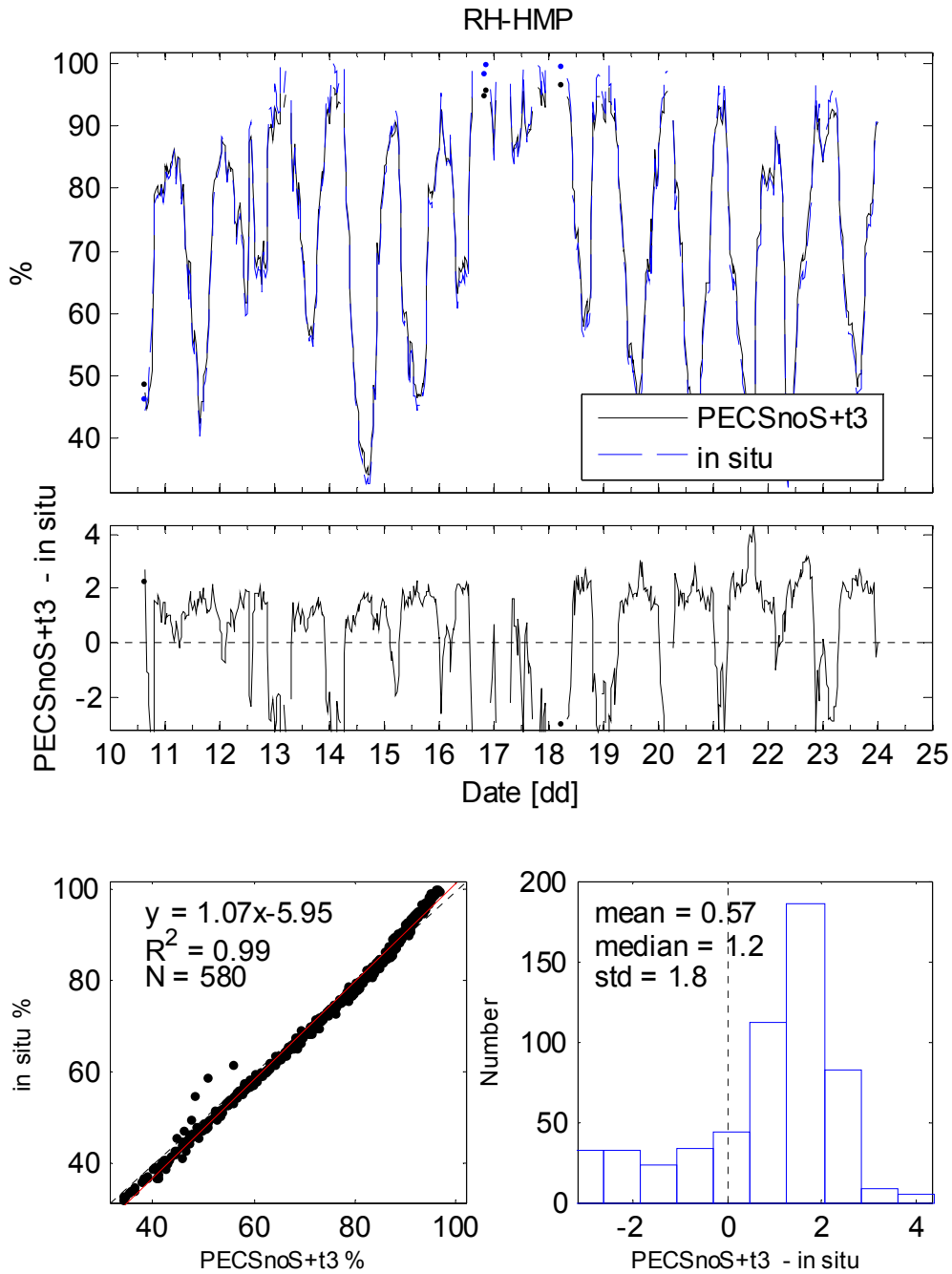


Figure 33 – Relative humidity measured with the PECS2 HMP155 and the *in situ* HMP45 temperature and relative humidity probes.

Site Name: Vaira Ranch – Ione (US-Var)

Visit Dates: 10 – 24 April 2017

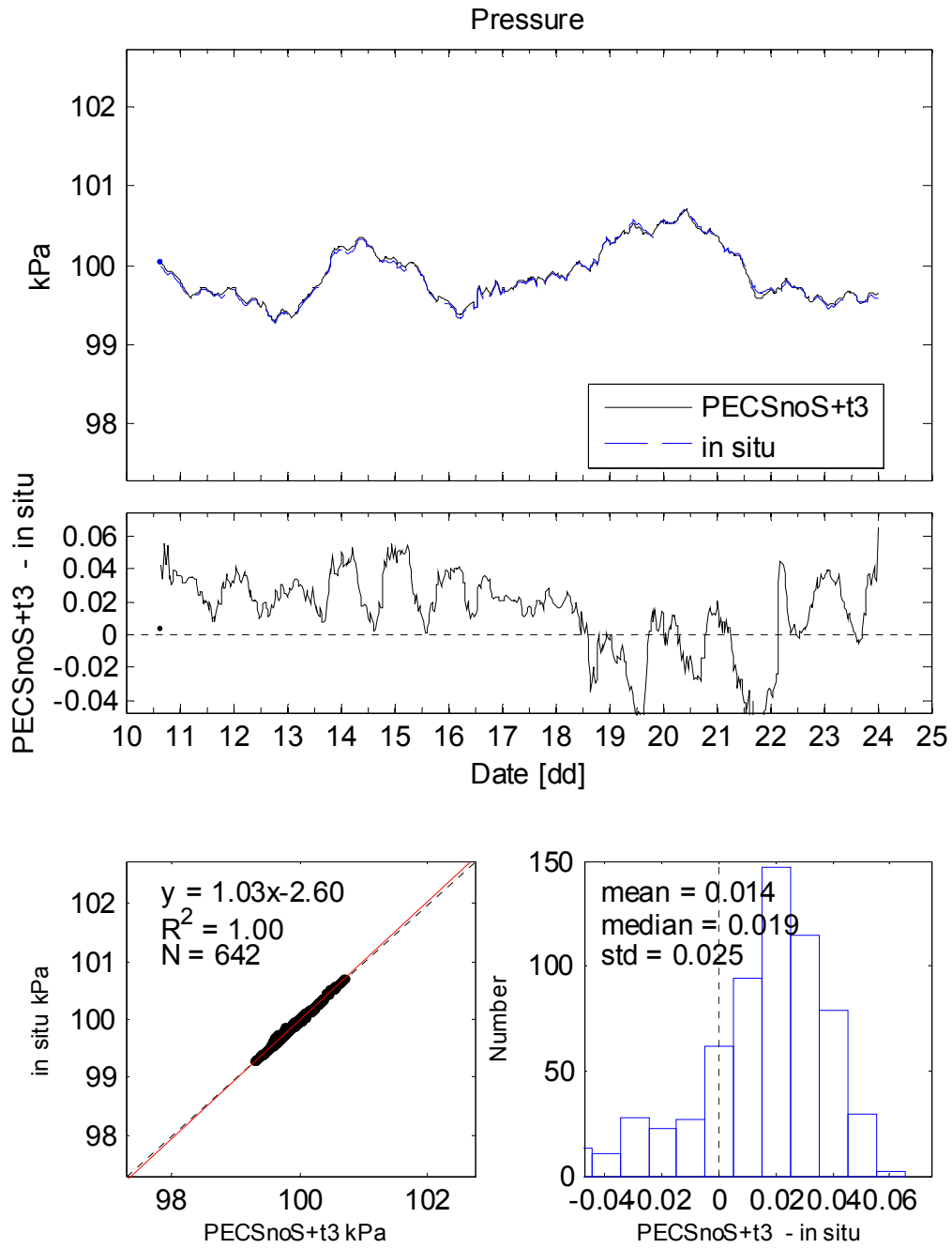


Figure 34 – Atmospheric pressure.

Site Name: Vaira Ranch – Ione (US-Var)  
Visit Dates: 10 – 24 April 2017

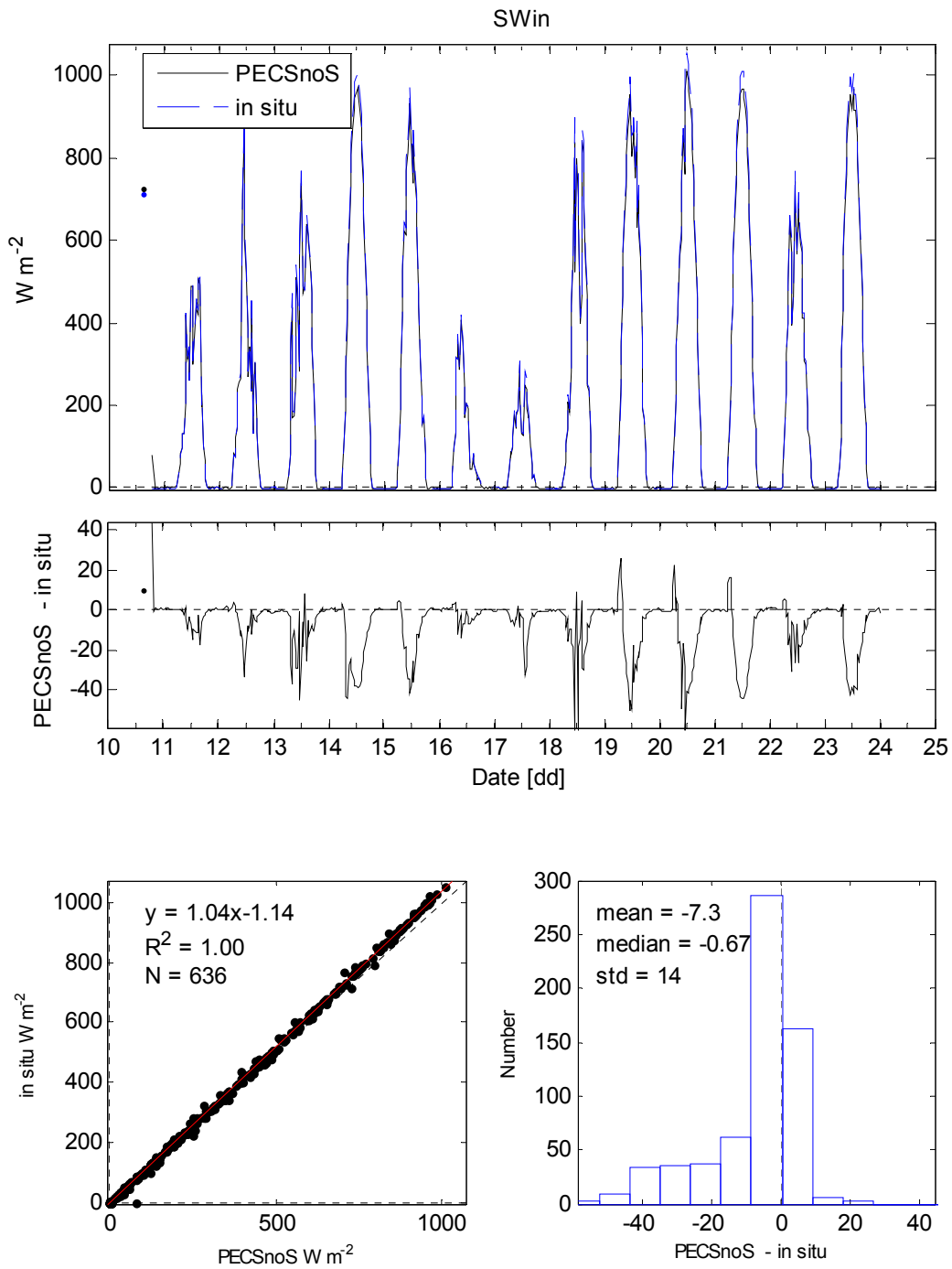


Figure 35 – Incoming shortwave radiation measured with the PECS2 CNR4 and the *in situ* CNR1.

Site Name: Vaira Ranch – Ione (US-Var)  
Visit Dates: 10 – 24 April 2017

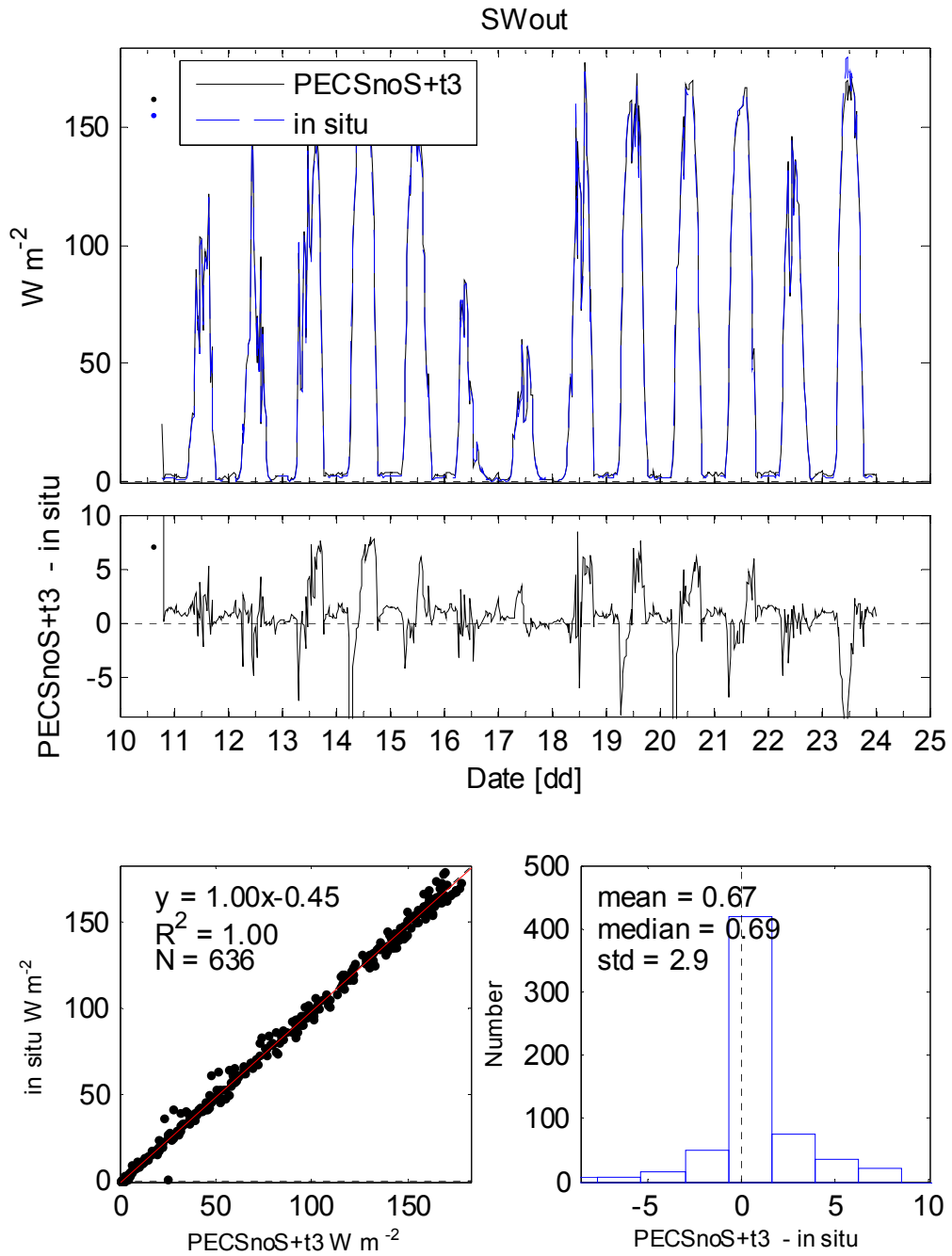


Figure 36 – Outgoing shortwave radiation measured with the PECS2 CNR4 and the *in situ* CNR1.

Site Name: Vaira Ranch – Ione (US-Var)  
Visit Dates: 10 – 24 April 2017

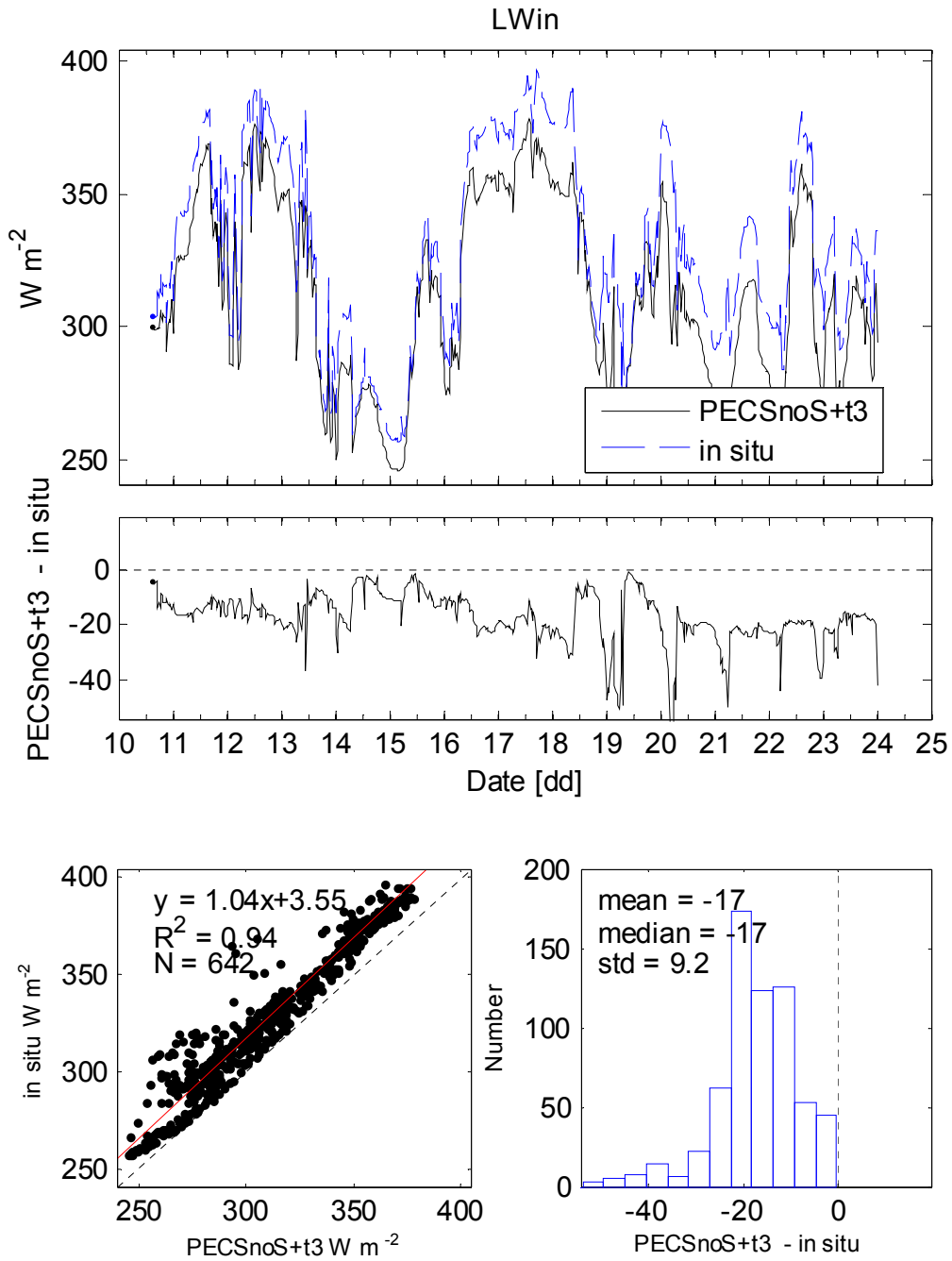


Figure 37 – Incoming longwave radiation measured with the PECS2 CNR4 and the *in situ* CNR1.

Site Name: Vaira Ranch – Ione (US-Var)

Visit Dates: 10 – 24 April 2017

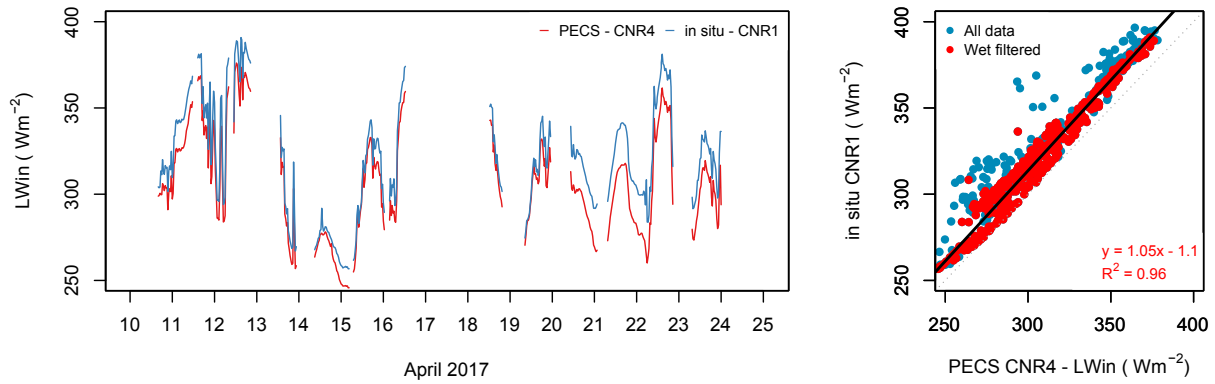


Figure 38 – Incoming longwave radiation measured with the PECS2 CNR4 and the *in situ* CNR1, separated by weather conditions. Regression line and statistics in the right panel apply to the rain filtered data.

Site Name: Vaira Ranch – Ione (US-Var)

Visit Dates: 10 – 24 April 2017

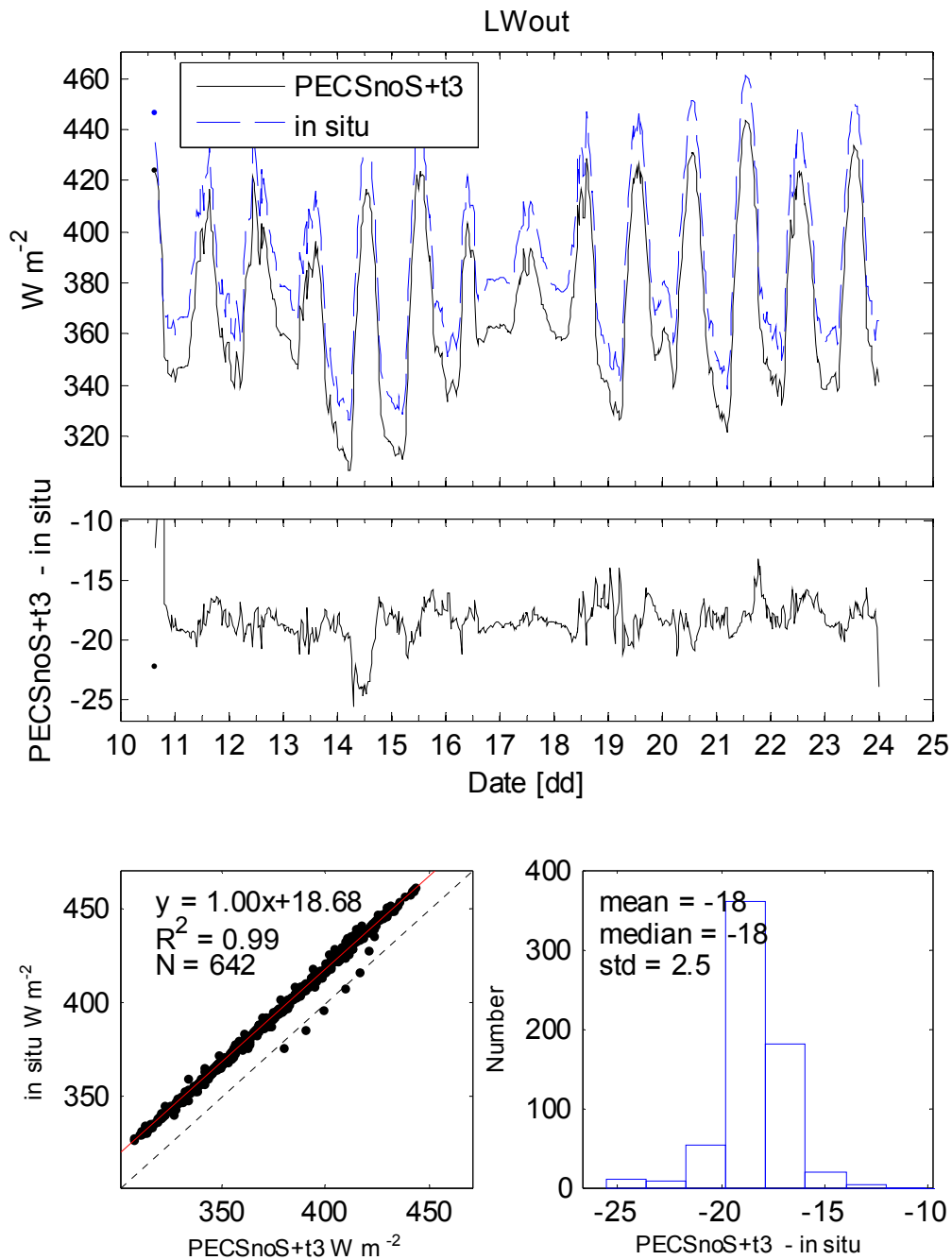


Figure 39 – Outgoing longwave radiation measured with the PECS2 CNR4 and the *in situ* CNR1.

Site Name: Vaira Ranch – Ione (US-Var)

Visit Dates: 10 – 24 April 2017

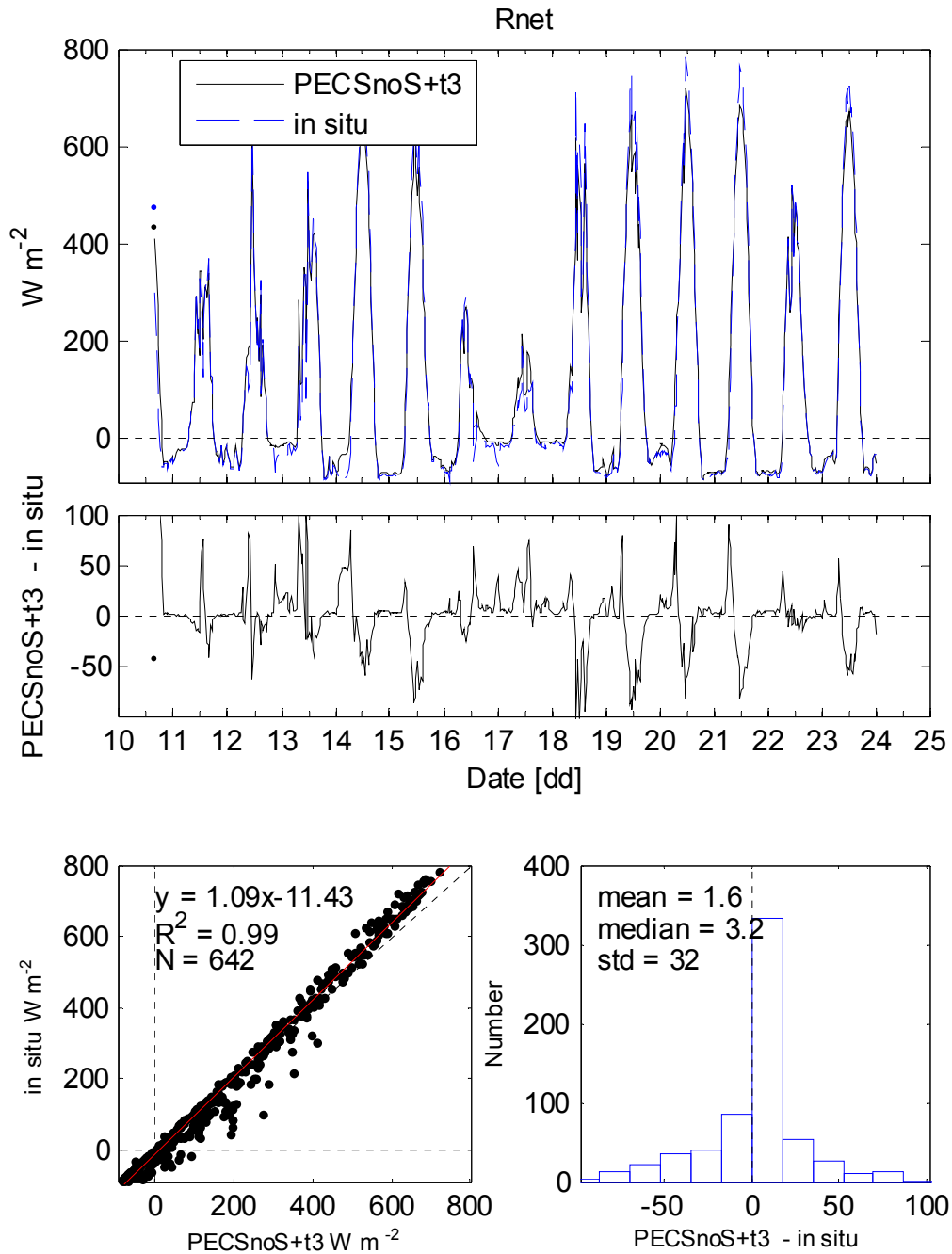


Figure 40 – Net radiation measured with the PECS2 CNR4 and the *in situ* NR Lite.

Site Name: Vaira Ranch – Ione (US-Var)

Visit Dates: 10 – 24 April 2017

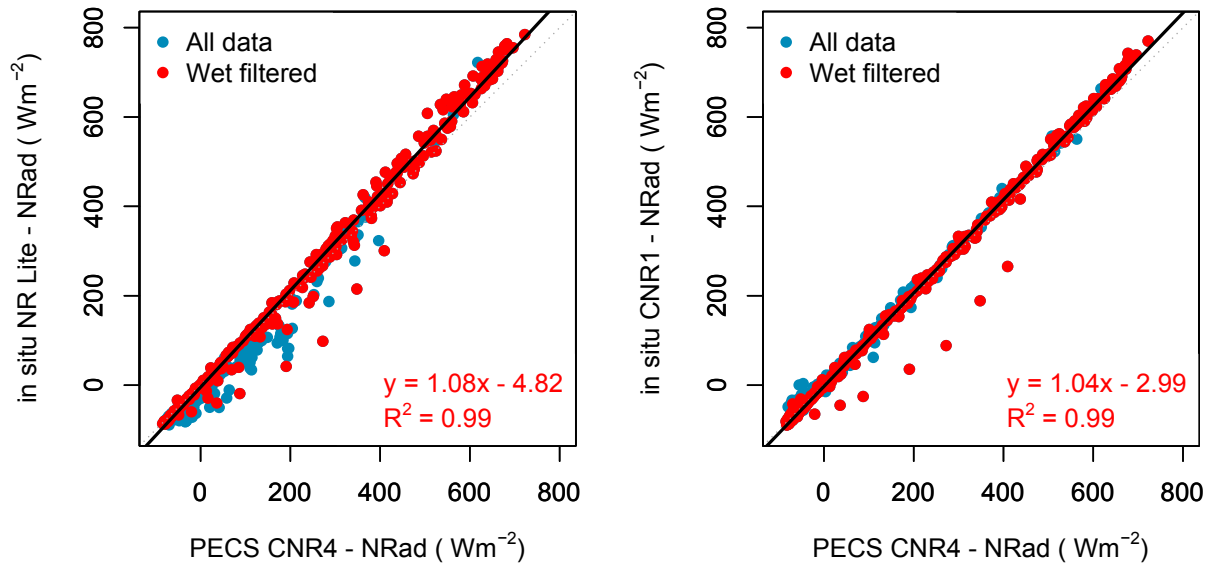


Figure 41 – Net radiation measured with the PECS2 CNR4 and the *in situ* NR Lite and the *in situ* CNR1 together with the rain filtered values. Both orthogonal regression lines and statistics apply to the rain filtered data.

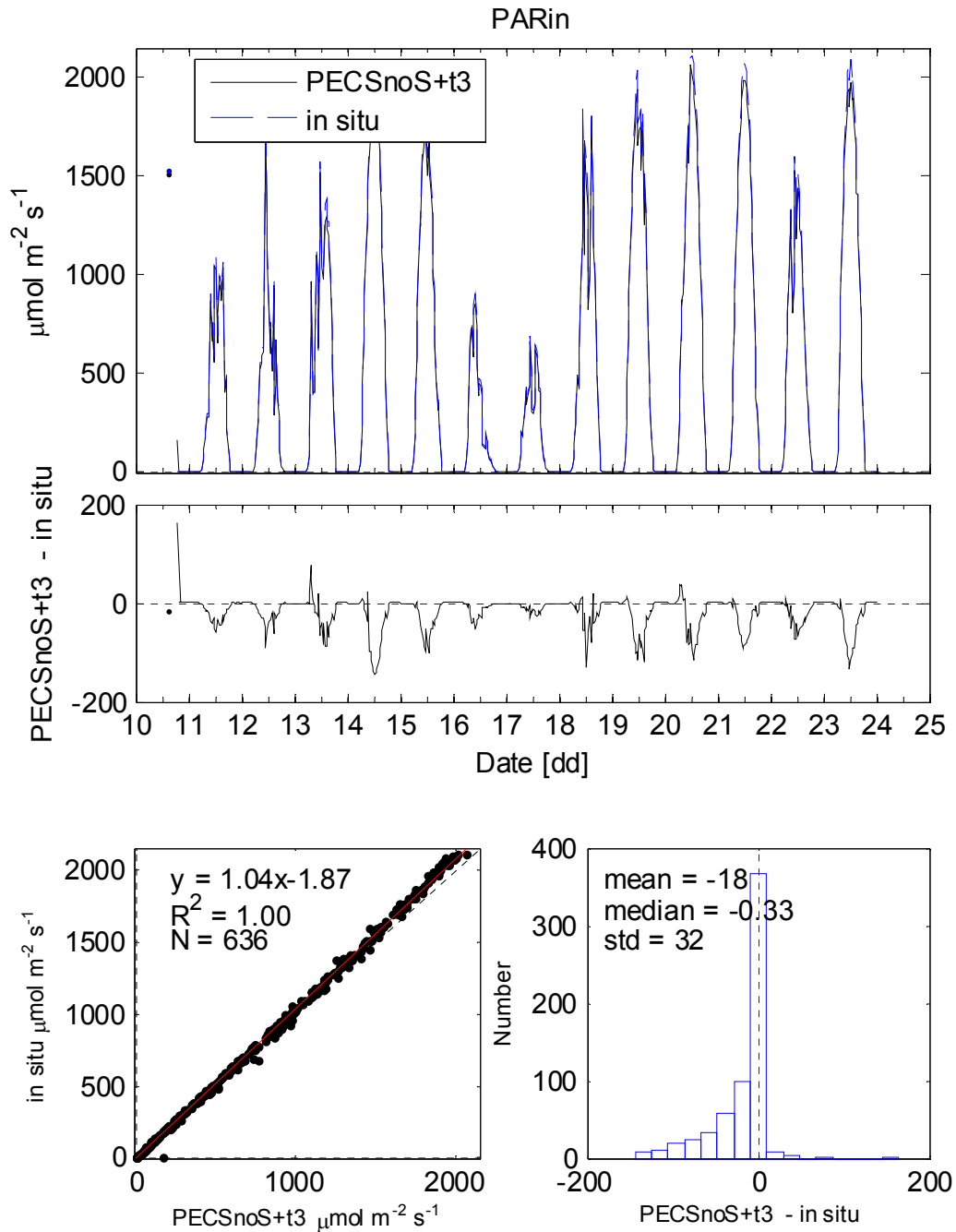


Figure 42 – Incoming photosynthetically active radiation (PAR).

Site Name: Vaira Ranch – Ione (US-Var)  
Visit Dates: 10 – 24 April 2017

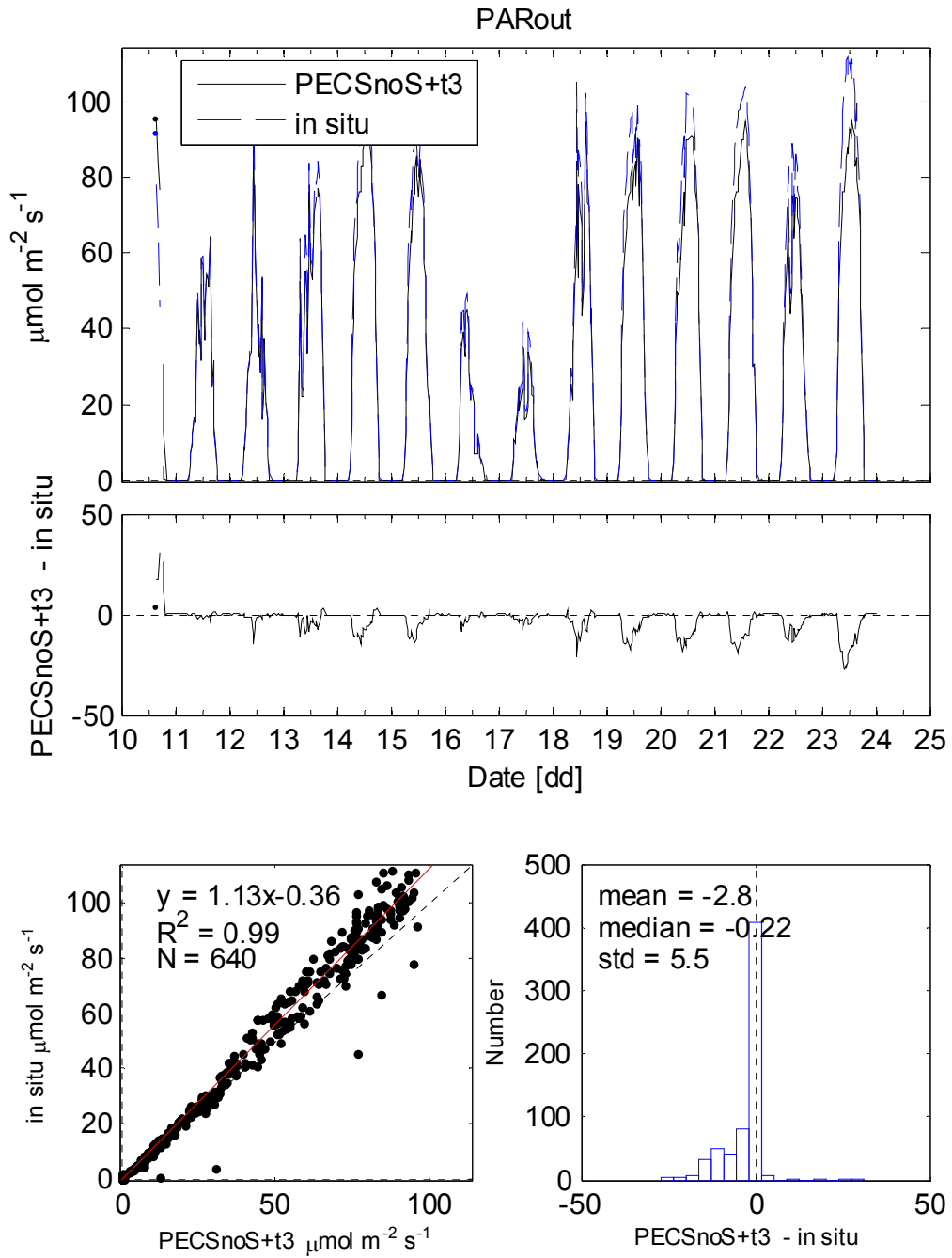


Figure 43 – Outgoing photosynthetically active radiation (PAR).

Site Name: Vaira Ranch – Ione (US-Var)

Visit Dates: 10 – 24 April 2017

Table 1 – Summary of basic statistics from linear regression and for each system of compared variables.

Fig # (*)	slope2	int2	R <sup>2</sup> 2	slope3	int3	R <sup>2</sup> 3	N	mean1	std1	max1	min1	mean2	std2	max2	min2	mean3	std3	max3	min3
6: CO2 flux	0.95	0.14	0.91				394	-4.36	8.58	12.67	-20.60	-3.98	8.13	11.71	-18.80				
9: Latent heat	0.92	1.12	0.97				393	92.36	102.81	365.14	-14.61	86.04	94.64	330.59	-15.73				
11: Sensible heat	1.08	-2.06	0.93				390	25.60	51.88	155.69	-59.98	25.51	55.73	175.94	-96.86				
13: u star	1.04	0.00	0.88				394	0.17	0.10	0.47	0.02	0.17	0.10	0.57	0.02				
29: Ts	0.81	5.08	0.96				394	17.23	3.58	24.80	6.00	19.03	2.91	25.33	11.47				
26: std(u_{rot})	1.01	-0.01	0.98				394	0.60	0.31	1.54	0.09	0.59	0.31	1.52	0.10				
27: std(v_{rot})	1.03	-0.02	0.98				394	0.63	0.37	2.25	0.11	0.63	0.38	2.57	0.13				
28: std(w_{rot})	0.99	0.00	0.99				394	0.23	0.13	0.59	0.03	0.22	0.12	0.59	0.03				
30: std(Ts)	1.03	0.01	0.94				389	0.45	0.21	1.46	0.06	0.47	0.22	1.19	0.08				
18: CO_2				0.99	0.07	1.00	397	17.52	1.21	20.26	15.85					17.37	1.19	20.10	15.72
19: std(CO_2)	0.95	-0.02	0.97	0.96	0.00	0.97	396	0.22	0.16	1.07	0.02	0.19	0.15	1.15	0.02	0.21	0.15	1.17	0.02
20: H_2O				0.98	15.10	0.99	396	466.83	81.85	686.95	250.32					471.45	80.02	689.39	259.89
21: std(H_2O)	0.99	-0.27	0.99	0.95	0.15	0.99	396	20.56	14.94	80.66	0.58	20.06	14.78	83.78	0.72	19.79	14.25	83.30	0.79
12: w'T'	0.97	0.00	0.94	1.06	-0.00	0.94	398	0.03	0.05	0.14	-0.05	0.02	0.05	0.15	-0.08	0.03	0.05	0.16	-0.08
7: w'CO_2'	0.70	0.00	0.91	0.98	0.00	0.93	397	-0.01	0.01	0.01	-0.03	0.00	0.01	0.01	-0.02	-0.01	0.01	0.01	-0.03
10: w'H_2O'	0.97	0.01	0.97	0.92	0.03	0.97	393	2.00	2.21	8.02	-0.33	1.94	2.14	7.54	-0.35	1.89	2.05	7.23	-0.37
31: Ta-HMP	1.04	-0.17	1.00				642	13.25	4.02	23.37	2.37	13.65	4.19	24.42	2.53				
32: RH-HMP	1.07	-5.95	0.99				580	72.92	16.67	96.81	34.12	72.35	17.90	99.94	32.05				
34: Pressure	1.03	-2.60	1.00				642	99.88	0.34	100.71	99.30	99.87	0.35	100.72	99.28				
23: Wind spd	1.04	-0.05	0.98				640	1.17	0.70	3.98	0.08	1.18	0.73	3.91	0.08				
22: Wind dir	1.02	27.34	1.00				628	151.04	99.93	358.54	2.58	174.97	100.59	356.51	5.69				
35: SWin	1.04	-1.14	1.00				636	217.86	299.67	1010.44	-4.42	225.11	311.21	1051.20	-3.25				
36: SWout	1.00	-0.45	1.00				636	46.80	58.15	177.49	-0.15	46.12	57.87	179.25	0.08				
37: LWin	1.04	3.55	0.94				642	313.01	34.78	378.22	245.67	330.44	36.27	396.50	256.73				
39: LWout	1.00	18.68	0.99				642	370.21	31.59	443.32	306.93	388.48	31.55	461.41	326.78				
40: Rnet	1.09	-	0.99				642	115.38	217.37	722.33	-84.28	113.78	235.77	784.61	-89.16				

Site Name: Vaira Ranch – Ione (US-Var)

Visit Dates: 10 – 24 April 2017

		11.43																	
Fig # (*)	slope2	int2	R <sup>2</sup> 2	slope3	int3	R <sup>2</sup> 3	N	mean1	std1	max1	min1	mean2	std2	max2	min2	mean3	std3	max3	min3
42: PARin	1.04	-1.87	1.00				636	454.46	613.98	2063.64	0.00	472.39	640.73	2109.60	-0.26				
43: PARout	1.13	-0.36	0.99				640	24.94	31.66	95.83	0.00	27.73	35.64	111.75	-0.31				

(\*) Variables marked “slope2”, “int2”, “R<sup>2</sup>2” represent regression coefficients between PECS2 and *in situ* values, while “slope3”, “int3”, “R<sup>2</sup>3” those between PECS2 and independently processed *in situ* values. At the same time columns headed with “mean1”, “std1”, “max1”, “min1”, “mean2”, “std2”, “max2”, “min2” and “mean3”, “std3”, “max3”, “min3”) correspond to values originating from the PECS2 (1), *in situ* (2) and independently processed (3) *in situ* values, respectively.

Site Name: Vaira Ranch – lone (US-Var)

Visit Dates: 10 – 24 April 2017

## Appendix 1 – Site information

### General Site Information

**Site Instrumentation (make/model)** - heights recorded below

Instrument	Make/model
Sonic anemometer	Gill Windmaster (x2)
Fast temperature sensor	
IRGA#1 (closed)	LI-7500
IRGA#2 (open/closed)	LI-7500
Other gas analyzer (describe)	
Radiometer#1 (specify net or which component)	CNR1
Radiometer#2 (specify net or which component)	NR-Lite
Radiometer#3 (specify net or which component)	
PAR#1	Kipp & Zonen (x2)
PAR#2	BF3
Temp. sensor #1 (is aspirated?)	HMP45
Temp. sensor #2 (is aspirated?)	
Humidity sensor (is aspirated?)	
Barometer	???. LI-7500
Wind sensor	
Vertical profile systems (temperature, winds, trace gases)	
Miscellaneous sensors (describe)	Rain gauge (Trelog, Geonor) (?)
Miscellaneous sensors (describe)	

**Eddy covariance details** (sensor heights, orientation, and separation)

	PECS	in-situ
<b>Sonic anemometer</b>	Gill R3-50	Gill Windmaster Pro (x2)
height [m]	2.12 m	2.02 m (x2)
orientation of sensor [o]	354	0 (x2)
distance from tower/tripod [m]	? m	n/a
orientation of boom (if different) [o]	0	n/a
<b>Open-path IRGA</b> (measure relative to sonic)	LI-7500A	LI-7500 (old)
Vertical separation [cm] (pos if IRGA is above sonic)	-13	-2
E/W separation [cm] (pos if IRGA is east of sonic)	+23	+22
N/S separation [cm] (pos if IRGA is north of sonic)	-5	-11
<b>Closed-path IRGA</b> (measure relative to sonic)	LI-7200	LI-7500 (new)

Site Name: Vaira Ranch – lone (US-Var)

Visit Dates: 10 – 24 April 2017

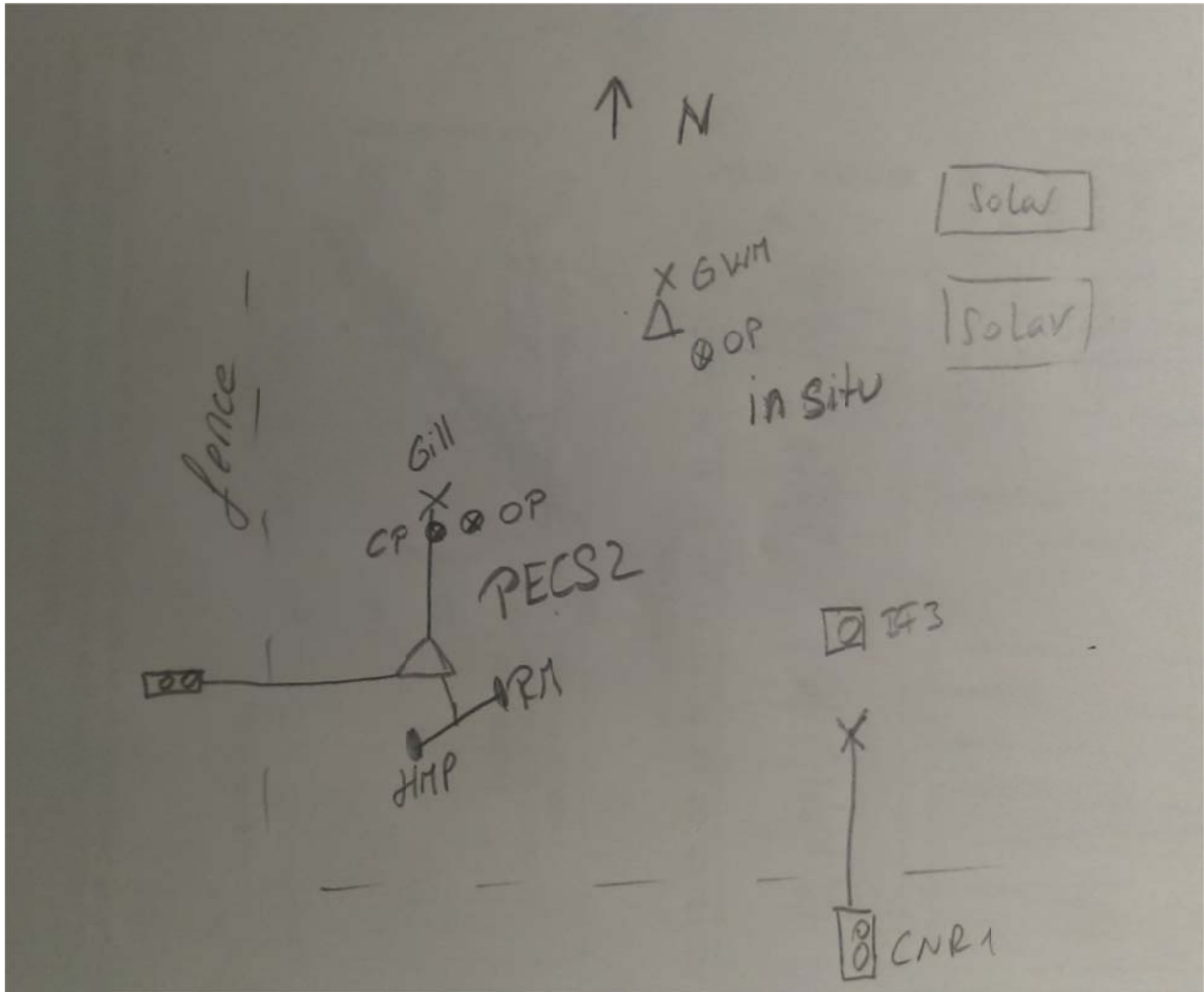
Vertical separation [cm] (pos if IRGA is above sonic)	-0	-2
E/W separation [cm] (pos if IRGA is east of sonic)	+5	+22
N/S separation [cm] (pos if IRGA is north of sonic)	-8	0
Inlet tube length [cm]	std	
Inlet tube inner diameter [mm]	std	
Inlet tube flow rate [lpm]	std	

**Slow response details** (sensor heights, orientation, and separation)

	<b>PECS</b>	<b>in-situ</b>
Radiometer#1 - height [m]	CNR4, 2.35 m	CNR1, 2.60 m
Radiometer#1 - orientation [o]	242	160
Radiometer#2 - height [m]		NR-Lite, 2.60 m
Radiometer#2 - orientation [o]		160
PAR - height [m]	2.35 m	approx. 2.60 m
PAR - orientation [o]	242	160
Temp. sensor#1 - height [m] (Asp)	1.77 m	
Temp. sensor#2 - height [m] (HMP)	2.05 m	2.0 m (HMP45)
Humidity sensor - height [m]	2.05 m	2.0 m (HMP45)
Pressure sensor height [m]	0.5 (main box), LI-7500	??? & LI-7500
Wind sensor - height [m]		
Direct/Diffuse Radiometer		BF3, 1.22 m

Site Name: Vaira Ranch – Ione (US-Var)  
Visit Dates: 10 – 24 April 2017

**Sketch layout of setup**



Site Name: Vaira Ranch – Ione (US-Var)  
Visit Dates: 10 – 24 April 2017

Appendix 2 – Photograph of Vaira Ranch site

